Growth of fluctuations in Chaplygin gas cosmologies:
A nonlinear Jeans scale for unified dark matter

Abdelrahman Abdullah[*] and Amr A. El-Zant[†]

Centre for Theoretical Physics, The British University in Egypt, Sherouk City 11837, Cairo, Egypt

Ali Ellithi

Physics Department, Faculty of Science, Cairo University, Cairo 12613, Egypt

Unified dark matter cosmologies economically combine missing matter and energy in a single fluid. Of these models, the standard Chaplygin gas is theoretically motivated, but faces problems in explaining large scale structure if linear perturbations are directly imposed on the homogeneous fluid. However, early formation of a clustered component of small halos is sufficient (and necessary) for hierarchical clustering to proceed in a cold dark matter (CDM) component as in the standard scenario, with the remaining homogeneous component acting as dark energy. We examine this possibility. A linear analysis shows that a critical Press-Schechter threshold for collapse can generally only be reached for generalized Chaplygin gas models that mimic ΛCDM, or ones where superluminal sound speeds occur. However, the standard Chaplygin gas case turns out to be marginal, with overdensities reaching order one in the linear regime. This motivates a nonlinear analysis. A simple infall model suggests that collapse is indeed possible for perturbations of order 1 kpc and above; for, as opposed to standard gases, pressure forces decrease with increasing densities, allowing for the collapse of linearly stable systems. This suggests that a cosmological scenario based on the standard Chaplygin gas may not be ruled out from the viewpoint of structure formation, as often assumed. On the other hand, a "nonlinear Jeans scale," constricting growth to scales $R \gtrsim$ kpc, which may be relevant to the small scale problems of CDM, is predicted. Finally, the background dynamics of clustered Chaplygin gas cosmologies is examined and confronted with observational datasets. It is found to be viable (at 1-sigma), with a mildly larger H_0 than ΛCDM, if the clustered fraction is larger than 90%.

I. INTRODUCTION

If general relativity holds on galactic and cosmological scales, the vast majority of the matter and energy content of our Universe must be in unknown form. In the standard "double dark" scenario, most of the dark sector is composed of dark energy in the form of a cosmological constant (Λ), while the rest is in a cold dark matter (CDM) component [1,2]. On the phenomenological level, the model is highly predictive and successful, the tension between the locally measured values of the expansion rate and that inferred from the cosmic microwave background (CMB) [3] notwithstanding. Other issues include small (galactic) scale problems at low redshift [4–6] and apparent discrepancies related to unexpectedly early galaxy, massive galaxy, and black hole formation [7–20].

On the fundamental level, despite extensive direct and collider searches, the prime CDM candidate, the weakly interacting massive particle (WIMP) believed to naturally arise in extensions of the standard model, has not materialized. The parameter range open to the "WIMP miracle" has been thus shrinking, at the same time that solutions to the aforementioned small scale problems have been invoking alternative dark matter candidates, such as warm dark matter [21–25], self-interacting dark matter [26–31], dissipative dark matter [32–35], and fuzzy dark matter made of ultralight axions [36–40]. Dark energy, on the other hand, remains evermore elusive. Particularly perplexing is its small magnitude and its relatively recent domination of the cosmic energy budget. These issues have been the subject of intense investigation, seeking alternatives to the cosmological constant as drivers of late cosmic acceleration, including modifications of fundamental gravitational law (e.g., [41–43] for reviews).

Dark energy effectively contributes a negative pressure term in the Friedmann acceleration equation, thus accelerating the late background dynamics. Earlier on, when the

---

[*]Also at Physics Department, Faculty of Science, Cairo University, Cairo, Egypt.
[†]amr.elzant@bue.edu.eg

083524-1

Universe was denser, the dark energy contribution was small; with radiation, pressureless matter dominates. Matter also dominates in the late Universe on nonlinear scales, of galaxies, and clusters, which are likewise characterized by relatively high density and little pressure. It is therefore natural to ask whether the double dark sector is simply composed of a single component, one with negative pressure at low density and essentially zero pressure at high densities.

The most extensively studied among unified dark matter models that fit the bill are generalized Chaplygin gas cosmologies [44,45], where the associated fluid comes with an equation of state relating the pressure and densities,

$$p = -\frac{Ac^2}{\rho^\alpha}, \qquad (1)$$

and where A and α are parameters that may be determined empirically to fit observations. Attractive aspects of such models include the simplicity via which the dark sector is unified through Eq. (1); their relevance to some problems affecting the standard model, such as the H_0 tension, is also of interest [46]. The original Chaplygin gas model, with $\alpha = 1$, is particularly well motivated from a theoretical point of view [47,48]. However, in its context, large scale perturbations, growing relatively late on a homogeneous background, are affected by the increasing sound speed in the expanding medium. The propagation rate of pressure forces thus catches up with the rate of gravitational collapse and halts the condensation. The perturbations thus become Jeans stable, oscillating acoustically and (Hubble) damping instead of growing. This imprints strong unobserved signatures on the matter density fluctuation power spectrum. The predictions regarding structure formation are, in this context, in catastrophic tension with observations [49].

Including a baryonic component improves the situation [50]. Nevertheless, values of α very close to zero (and therefore to the standard model) or greater than one (when the sound speed may become superluminal) are still favored [51–53]. Indeed, combinations of supernova data, CMB, and baryon acoustic oscillations data appear to conclusively constrain Chaplygin gas cosmologies to the neighborhood of ΛCDM [54,55]. Nonadiabatic perturbations (e.g., [56–58]) were also considered. It is not clear, however, whether the growth of such perturbations would remain impervious to pressure forces into the nonlinear regime.

One may immediately remark, however, that the above constraints are inferred by considering a nearly homogeneous Chaplygin gas that remains unclustered on all scales, including the smallest ones (corresponding to dwarf galaxy halos and smaller). For example, Sandvik *et al.* [49] examine linear perturbations in a homogeneous Chaplygin gas fluid on scales corresponding to comoving wave numbers $k < 1$ Mpc^{-1}. However, in a hierarchical

scenario, the medium in which such perturbations are probed should not be considered homogeneous. Indeed, in the standard CDM pictures it has already clustered on a hierarchy of smaller scales, from the smallest Earth mass gravitationally bound structures up to galactic and cluster scale halos.

In a successful unified dark matter scenario, large scale perturbations would occur in an already clustered medium. Such a medium would act as pressureless CDM, readily allowing further clustering. The hierarchically forming halos would host galaxies with spatial distribution that may be expected to be quite close to the standard CDM case, with a commensurately similar linear matter power spectrum. Furthermore, if clustering is efficient, simple arguments suggest that the background evolution can also be rendered compatible for observations, even for the theoretically attractive case of $\alpha = 1$ [59].

The central question is therefore not whether the evolution of large scale (and thus late growing) perturbations in a homogeneous unified dark matter fluid is compatible with data, but whether such a medium can sufficiently cluster early on. For this would enable it to exhibit a significant CDM-like component, which can hierarchically condense into halos and hence host galaxies. Answering this in full requires, in principle, detailed modeling of the nonlinear collapse and clustering process. This has not been available, due to the novelty and presumed complexity of modeling the hydrodynamics of fluids with anomalous equations of state, involving negative pressure with absolute value decreasing with density. However, this anomalous form itself suggests that examining the nonlinear regime must be considered central to any investigation because, in a Chaplygin gas, pressure forces become less significant with increasing density and a linearly (Jeans) stable system may be nonlinearly unstable against gravitational collapse, providing for a medium of collapsed halos that may cluster hierarchically. This is in stark contrast to a regular gas, where the sound speed and pressure forces necessarily increase with density, which in turn implies that a Jeans stable gas generally remains stable against nonlinear perturbations. Pending full hydrodynamic treatment, estimates of the effect of nonlinearity, circumventing complications of unknown hydrodynamics while capturing the essentials, thus seem crucial to adequately evaluating the efficacy of Chaplygin gas cosmology.

Here we revisit the linear and nonlinear stability of generalized Chaplygin gases, with the aforementioned remarks in mind. We confirm previous results suggesting that linear clustering is most efficient for either very small values of α in Eq. (1) or larger ones associated with superluminal sound speeds (Sec. II). Nevertheless, we point out that even a linear analysis predicts that perturbations can come tantalizingly close (at small scales) to the critical (Press-Schechter-based value) for collapse in the fiducial

case of standard Chaplygin gas with $\alpha = 1$. This further motivates examination of the nonlinear regime. In Sec. III, we review some previous attempts at such an analysis, before proceeding to estimate the importance of pressure forces along an inhomogeneous spherical collapse model, avoiding complications that come with shell crossing and possible formation of shocks. In Sec. IV, we discuss the basic characteristics and viability of the background evolution of a clustering Chaplygin gas cosmology.

II. PERTURBATIONS IN THE LINEAR REGIME

We briefly review the evolution of the homogeneous generalized Chaplygin gas and the fixing of its parameters. We then describe the effect of perturbations and present the resulting matter power spectra and associated rms mass fluctuations on various scales.

A. Background evolution of homogeneous Chaplygin gases

By inserting the equation of state (1) into the energy conservation law

$$\dot{\rho} + 3H(\rho + p/c^2) = 0, \tag{2}$$

where H is the Hubble parameter, one obtains the evolution equation for the homogeneous generalized cosmological Chaplygin gas,

$$\rho(t) = \left[A + \frac{B}{a^{3(1+\alpha)}}\right]^{\frac{1}{1+\alpha}}. \tag{3}$$

Here, $a(t)$ is the scale factor and A and B are constants that can be related to the dark energy and matter cosmic contents, respectively,

$$A = \rho_c^{1+\alpha}(1 - \Omega_m^{1+\alpha}), \qquad B = \rho_c^{1+\alpha}\Omega_m^{1+\alpha}, \tag{4}$$

where ρ_c is the current total density, which is thus assumed to correspond to the critical closure density, and $\Omega_m = \rho_m/\rho_c$ is the current ratio of matter to total density [60]. For sufficiently small a, the second term is dominant in (3) and behaves as $\rho \sim 1/a^3$, in correspondence to the standard matter domination era. On the other hand, the current dark energy dominated era is characterized by

$$\rho(a = 1) = \rho_c = (A + B)^{\frac{1}{1+\alpha}}, \tag{5}$$

while $\rho \to A^{\frac{1}{1+\alpha}}$ specifies the dark energy content. In turn, for a given α, A, and B may be fixed by specifying the current contribution of the dark energy and matter components to the total energy density.

B. Growth and oscillation of linear perturbations

The relativistic equation that describes the growth of small matter overdensity perturbation modes in a nearly homogeneous fluid may be written as

$$\ddot{\delta}_k + H\dot{\delta}_k[2 - 3(2w - c_s^2)] - \frac{3}{2}H^2\delta_k[1 - 6c_s^2 + 8w - 3w^2]$$
$$= -\left(\frac{kc_s}{a}\right)^2\delta_k, \tag{6}$$

where the equation of state parameter w and the sound speed c_s are given by

$$w \equiv \frac{p}{\rho} = -\left[1 + \frac{\Omega_m^*}{1 - \Omega_m^*}a^{-3(1+\alpha)}\right]^{-1} \tag{7}$$

and

$$c_s^2 \equiv \frac{\partial p}{\partial \rho} = -\alpha w c^2, \tag{8}$$

with $\Omega_m^* = \Omega_m^{1+\alpha}$ and Ω_m the current matter density parameter [49]. In Eq. (6), c_s is assumed to be expressed in units of $c = 1$.

Equation (6) is solved numerically by changing the independent variable from t to $\ln a$. Accordingly,

$$\frac{d}{dt} = H\frac{d}{d\ln a}, \tag{9}$$

and

$$\dot{\delta}_k = H^2\delta'' + \frac{1}{2}(H^2)'\delta', \tag{10}$$

where $' \equiv \frac{d}{d\ln a}$ and

$$\xi \equiv \frac{(H^2)'}{2H^2} = -\frac{3}{2}\left(1 + \left(\frac{1}{\Omega_{M*}} - 1\right)a^{3(1+\alpha)}\right)^{-1}. \tag{11}$$

Equation (6) can then be written as

$$\delta_k'' + [2 + \xi - 3(2w - c_s^2)]\delta_k'$$
$$= \left[\frac{3}{2}(1 - 6c_s^2 + 8w - 3w^2) - \left(\frac{kc_s}{aH}\right)^2\right]\delta_k. \tag{12}$$

We immediately note the appearance, in this context, of a (nonrelativistic) Jeans length, arising from the presence of the pressure term,

$$\lambda_J = \sqrt{\frac{\pi|c_s^2|}{G\rho}}. \tag{13}$$

As a result, if, as will be assumed here, $c_s^2 > 0$ ($\alpha > 0$), linear perturbations on scales below λ_J will acoustically

oscillate and damp with the expansion, rather than grow. (If $c_s^2 < 0$, the perturbations below the critical scale will grow exponentially [49,54].)

The Jeans length, as usual, reflects a competition between the sound crossing time and the gravitational collapse time, determined by the dynamical time $\approx (G\rho)^{-1/2}$. In the matter dominated regime, $\rho \propto 1/a^3$ and $c_s^2 \propto \alpha/\rho^{\alpha+1}$. For $\alpha > 0$ ($c_s^2 > 0$), λ_J is a real number that rapidly increases as

$$\lambda_J \propto \sqrt{\alpha} a^{3(\alpha+2)/2} \tag{14}$$

as the Universe expands. For $\alpha = 1$, for example, this corresponds to a steep increase $\sim a^{9/2}$. Thus, according to such estimates—derived on the assumption that the perturbed medium remains nearly homogeneous on scales smaller than λ_J—the growth of late forming structures is suppressed, unless α is very small; otherwise, the rate of gravitational collapse cannot catch up with the swiftly increasing sound horizon.

In this context, the large scale structure power spectrum will be dominated by acoustic oscillations, if perturbations on the relevant scales are evolved to the present while imprinted on a homogeneous background. If smaller scales have collapsed into halos, however, the situation is qualitatively different. For, in this case, a clustered CDM medium forms, composed of halos that may merge into larger structures, as in the standard scenario. This merging process, also as in the standard scenario, reflects the growth of larger scale perturbations, which are now imprinted on the clustered medium and not on the initial homogeneous background. As the clustered medium is made of high density halos, and is therefore essentially pressureless, it should act as a standard dark matter component and thus clusters on larger scales as CDM does. The rest of this study aims at investigating this possibility.

C. Power spectrum and rms fluctuations

We start with a standard Gaussian random field of density perturbations. It is obtained using the publicly available code CAMB [61], with cosmological parameters $h = 0.69$, $n_s = 1$, $\Omega_\Lambda = 0.71$, $\Omega_m = 0.29$, and $\Omega_k = 0.001$. This fixes our initial conditions at $z = 100$, when the Chaplygin gas pressure is still entirely negligible, and the cosmological model and its spectrum of fluctuations are indistinguishable from ΛCDM.

We then evolve realizations of this Gaussian random field by integrating Eq. (12), using an adaptive Runge-Kutta method, to obtain the matter power spectrum

$$P(k) = \langle |\delta(k)|^2 \rangle \tag{15}$$

at different redshifts. and also the associated dimensionless power spectrum,

$$\Delta^2(k) \equiv \frac{1}{2\pi^2} k^3 P(k), \tag{16}$$

which measures the contribution of perturbations per unit logarithmic interval at wave number k to the variance of matter density fluctuations. This variance may in turn be given in terms of the power spectrum, filtered on spatial scales R, such that

$$\sigma_M^2(R) = \frac{1}{2\pi^2} \int P(k) W_R^2(k) k^2 dk, \tag{17}$$

where $W_R(k)$ is the Fourier transform of the spatial filter (henceforth assumed top hat).

D. Results: Marginal stability at $\alpha = 1$

As expected from previous work and discussed in the Introduction, when the index α in (1) is small, the growth of perturbations in a homogeneous generalized Chaplygin gas is closest to the standard case involving CDM. Figure (1) shows the rms dispersion $\sigma_M(R)$ for the Chaplygin fluid for $\alpha = 10^{-5}$. Perturbations at all smaller scales pass the critical Press-Schechter threshold of about $\sigma_M = 1.7$ (e.g., [62]), the Jeans length catching up with the scale of the collapsing object only well into the nonlinear regime, when bound halos are expected to have already formed. The largest perturbation scale shown ($R = 10$ Mpc) remains largely unaffected by the generalized Chaplygin gas pressure. The effect of pressure forces in this case (of small α) is small due to the smallness of the prefactor α in the expression of the sound speed (8).

For large values of α, the suppression of structure formation is also alleviated. Here, the reduction is due to a steep variation of the sound speed with density. The results for $\alpha = 2$ are shown in Fig. 2. Note that here the
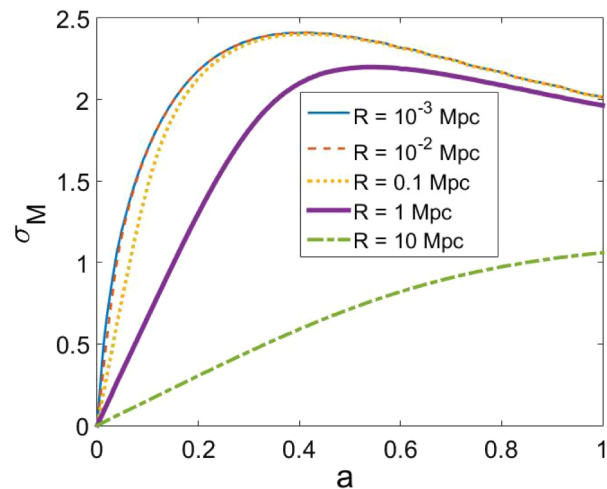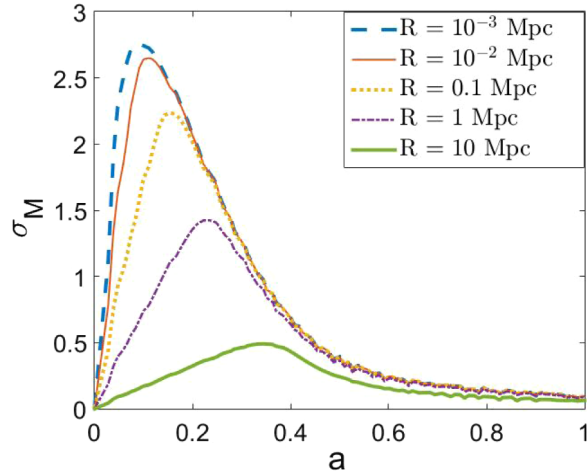

FIG. 1. The evolution of the mass dispersion $\sigma_M(R, a)$, with scale factor a, for a generalized Chaplygin gas with $\alpha = 10^{-5}$ [in Eq. (1)], smoothed on the indicated (comoving) scales R.
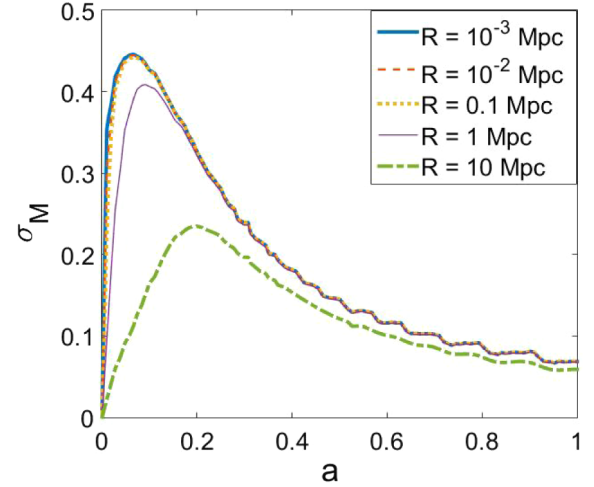
FIG. 2.   Mass dispersion $\sigma_M(R, a)$, when $\alpha = 2$ in Eq. (1).

FIG. 3.   Mass dispersion $\sigma_M(R, a)$ when $\alpha = 10^{-2}$ in Eq. (1).

Press-Schechter threshold of around 1.7 is only passed on scales smaller than 1 Mpc, as the steep dependence of the pressure on density enables the growth at higher redshift when the background density is relatively large. This is the epoch where smaller perturbations grow most, due to their earlier head start (resulting from the shape of the standard initial dimensionless power spectrum). The growth of larger fluctuations, which takes place later, is highly suppressed [as they evolve later, when the background density is lower and Jeans scale growing as in Eq. (14)]. The collapse of the smaller perturbations is nonetheless sufficient to allow for a pressureless clustered CDM component, from which higher scales can hierarchically cluster. However, the sound speed in the remaining homogeneous background fluid can become superluminal at lower redshift. Whether this is physically admissible has been discussed in [52].

Intermediate values of α correspond to situations whereby neither a steep decrease in sound speed with density nor small prefactor α in Eq. (8) may sufficiently suppress the pressure forces. Figure 3 shows the case $\alpha = 10^{-2}$, where all perturbations acoustically oscillate and damp well before reaching the critical Press-Schechter threshold of $\sigma_M = 1.7$. In this case, therefore, no structure is expected to form on any scale.

Of particular interest is the fiducial case of $\alpha = 1$. Here, the Press-Schechter threshold is not formally reached, but the necessary condition for nonlinear growth, $\sigma_M \approx 1$, is attained on the smaller scales shown, of $R \leq 0.1$ Mpc. This leaves open the possibility of collapse in the nonlinear regime, which is characterized by increased density and steeply decreased pressure, and with this, the emergence of a CDM component composed of collapsed halos and the possibility of hierarchical clustering thereof.

Further clarification of a possible route to hierarchical structure formation in such a situation (i.e., for the case $\alpha = 1$) may be illustrated by explicitly examining the evolution of the dimensionless power spectrum. This we plot in Fig. 5. As is clear, linear perturbations in the homogeneous fiducial Chaplygin gas universe at $z = 0$ ($a = 1$) are eventually acoustically suppressed at all scales. Nevertheless, as one goes back to earlier times (larger background ρ), significant growth can occur, before oscillations and expansion damping dominate. This gives rise to the peaks in the dispersion σ_M, which touch the nonlinear regime and approach the Press-Schechter collapse threshold in Fig. 4.

The marginal stability observed in the linear regime may have crucial consequences for the clustering of the Chaplygin gas, for the fiducial Chaplygin gas has the peculiar property that the pressure forces in general steeply decrease in magnitude with density: $\sim c_s^2/\rho \propto \sim 1/\rho^3$. Therefore, if collapse is so nearly reached in the linear context, it may very well actually occur if the nonlinear increase in density is adequately taken into account. This is
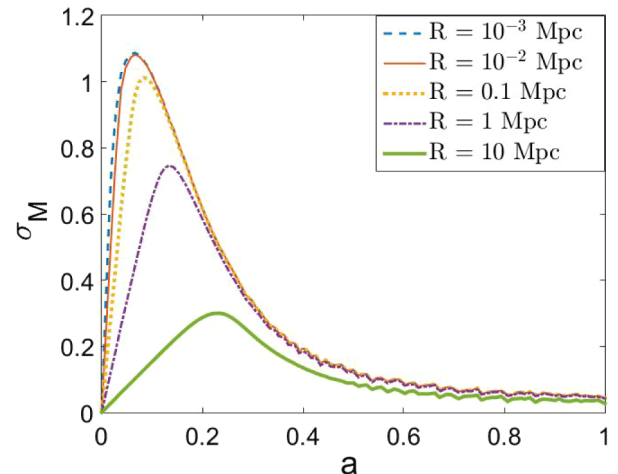
FIG. 4.   Mass dispersion $\sigma_M(R, a)$ for the case of the standard Chaplygin gas, with $\alpha = 1$ in Eq. (1).
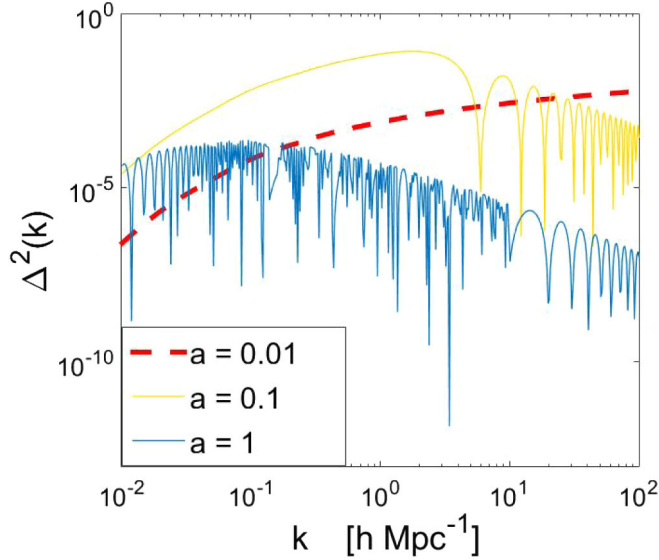
FIG. 5. The evolution, with scale factor, of the dimensionless power spectrum of linear perturbations in a standard Chaplygin fluid ($\alpha = 1$) cosmology.
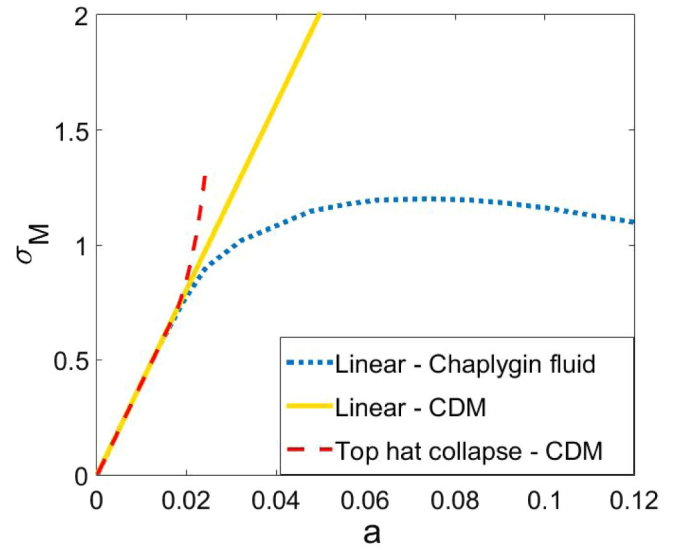

FIG. 6. The evolution, in the linear regime, of the mass dispersion $\sigma_M(R, a)$ on 1 kpc scale in the standard Chaplygin fluid, compared with the evolution of overdensity corresponding CDM case and its nonlinear (homogeneous) top hat counterpart.

what we attempt to investigate in the next section, by invoking a simple spherical infall model.

III. NONLINEAR REGIME: EXPECTED CLUSTERING FOR $\alpha = 1$ AND MINIMAL MASS SCALE

A. Motivation

In Fig. 6 we compare the linear growth of perturbations, on a kiloparsec scale, in a pressureless CDM fluid to that in the fiducial Chaplygin gas ($\alpha = 1$) and to the nonlinear growth in a homogeneous top hat collapse model of a pressureless medium (e.g., [62]). As is clear, the growths are similar up to $\sigma_M \approx 1$. Beyond that, as may be expected, the overdensity associated with nonlinear top hat collapse diverges from the linear one in the pressureless case. In the linear analysis, the overdensity growth in the Chaplygin gas case is then reversed, as the pressure term overtakes self-gravity in significance. Again, if one was dealing with a regular laboratory gas, this trend would be expected to be reinforced in the nonlinear regime, since the sound speed and associated pressure forces increase as the densities increase. At an overdensity of order one, however, the squared sound speed in a Chaplygin gas $c_s^2 = dp/dr \sim 1/\rho^2$ has already decreased by a factor of 4. This implies (for a given density gradient) an order of magnitude (a factor of 8 to be precise) decline in pressure forces $\frac{1}{\rho} dp/dr \sim \frac{c_s^2}{\rho}$. This is not taken into account in a linear analysis, which effectively assumes that the pressure inside the overdensity can be characterized by the steeply rising sound speed of the rapidly decreasing density of the expanding background. (Indeed, with $c_s^2/\rho \sim 1/a^9$.)

Further compression implies additional suppression of pressure forces, relative to the linear regime, while the competing gravitational forces are enhanced. Once turnaround is achieved, the pressure forces can only become less important, as the density now increases in absolute terms (and not only relative to the expanding background). It would therefore seem entirely plausible that a nonlinear analysis would predict collapse instead of reexpansion of small scale perturbations, allowing for halos that can hierarchically cluster as in the standard CDM-based scenario.

Given this, remarkably little work regarding the nonlinear stability of the Chaplygin gas has been carried out. Here, we briefly discuss a couple of examples, pointing out that the conclusions attained from the simplified treatments are far from conclusive. Given the complexity of the problem at hand, and the largely unexplored hydrodynamics of the peculiar equation of state involved, this is not surprising.

Bilić *et al.* [63] have used the continuity and Euler-Poisson system of equations in an expanding Universe to derive an equation that describes the growth of overdensity perturbations,

$$a^2\delta'' + \frac{3}{2}a\delta' - \frac{3}{2}\delta(1 + \delta) - \frac{4}{3}\frac{(a\delta')^2}{1 + \delta}$$
$$- \frac{1 + \delta}{a^2 H^2}\frac{\partial}{\partial x_i}\left(\frac{c_s^2}{1 + \delta}\frac{\partial\delta}{\partial x_i}\right) = 0, \qquad (18)$$

where a $'$ denotes the derivative with respect to scale factor a, $\mathcal{H}$ is a local Hubble parameter (describing the expansion or contraction rate of each shell inside a spherical

overdensity), and x is a radial variable. In order to study the nonlinear growth, a self-similar solution, involving a time-dependent scale R, such that $\delta(a, \mathbf{x}) = \delta_R(a) f(x/R)$, was proposed. It is not clear, however, that such a solution exists and for which form of f. This is crucial, as in the presence of significant pressure gradients, such a form may very well not in fact exist (even with gravity alone acting, they generally exist only for power law initial conditions [64]). In the aforementioned work, a Gaussian $f(x/R) = \exp(\frac{-x^2}{2R^2})$ was *a priori* assumed, and the equation arising from substituting the resulting $\delta(a, \mathbf{x})$ into (18) still involved the Gaussian and its derivatives. To get rid of it, the resulting equation was arbitrarily solved at $x = 0$. However, transforming a partial differential equation, describing fluid flow (and its continuity), into an ordinary one at an arbitrary point cannot be considered generically valid. It also appears that the background sound speed, and not the much smaller one inside the perturbation (as discussed above), was used. In turn, the principal conclusion from that work, which points toward inefficient Chaplygin gas clustering, even in the nonlinear regime, seems to lack sufficient foundation to rule out the viability of the otherwise appealing unified dark matter cosmologies based on the standard Chaplygin gas.

Another attempt at examining nonlinear growth in Chaplygin gases was undertaken by Fernandes *et al.* [65]. Here, a top hat collapse model was invoked, in such a way that a homogeneous density profile was assumed inside a spherical perturbation with a pressure discontinuity at the boundary, separating the overdense region from the homogeneous background. Thus, this ignores pressure gradients inside the perturbation and concentrates all pressure forces at the boundary. The results are also anomalous—and in disagreement with linear analysis—in the sense that they suggest that pressure forces associated with larger positive values of α tend to actually speed up the collapse relative to the pressureless case of $\alpha = 0$.

In the following, we describe a model that may help estimate the possibility of collapse and formation of self-gravitating halos in standard Chaplygin gas cosmologies. The principal goal is to take into account, in simplest terms, the effect of the peculiar phenomenon of the decrease in the magnitude of the pressure with the increasing (over)density, characteristic of any unified dark matter fluid.

B. Possibility and scale of unhindered collapse in a spherical infall model

1. Basic idea

To our knowledge, the hydrodynamics of a negative pressure gas has not been explored in any detail. In the mathematical literature, it is known that solutions of the Riemann problem lead to shocks [66–68], which may accompany eventual shell crossing in a nonlinear collapse model. In the following, we wish to circumvent

such complications, while obtaining a reasonably realistic estimate for the possibility of gravity overcoming pressure forces, so as to allow for collapse in the standard Chaplygin gas.

For this purpose, we use a simple spherical infall model, where, in the absence of pressure forces, all shells reach their maximum radius and turnaround before any shell crossing occurs. We solve the dynamics of the model and estimate the pressure forces along the unperturbed motion. Given that Chaplygin gas pressure forces necessarily become less important with increasing density, while gravitational forces become more potent, the maximum strength of the pressure forces to gravitational force, at every shell, will occur close to its maximum expansion at turnaround. In this context, if we can show that pressure forces are small compared to gravitational ones before and around the turnaround, for all shells, then this suggests they are negligible throughout the evolution and thus collapse akin what happens in the case of pressureless CDM may occur.

2. Model

In the context just set, we consider the dynamics of a pressureless matter perturbation in a flat, matter dominated universe. As we are interested in the early collapse of the smallest structures, when dark energy is not important, we limit ourselves to the case of an Einstein–de Sitter universe. Without shell crossing, the mass $M = M(< r)$, within a shell at radius r of a spherical perturbation, is conserved. The dynamics of its Lagrangian radius is then simply determined by $\ddot{r} = -GM/r^2$, with (specific) energy integral $\frac{1}{2}(\frac{dr}{dt})^2 - \frac{GM}{r} = E$, and parametric solutions in terms of a phase angle $0 \le \theta \le 2\pi$,

$$r = A_{\mathrm{sh}}(1 - \cos\theta),$$
$$t = B_{\mathrm{sh}}(\theta - \sin\theta), \tag{19}$$

where $A_{\mathrm{sh}} = GM/|E|$ and $A_{\mathrm{sh}}^3 = GMB_{\mathrm{sh}}^2$, and the subscripts indicate that these constants are specific to each shell. They can be fixed by conditions at time t_i, where the linear regime may be assumed to reign. The initial velocity of a shell corresponds to the cosmological expansion determined by the Hubble parameter H_i, minus a peculiar (inward) velocity term $\overline{\delta}_i(r_i) H_i r_i/3$. The initial average overdensity within radius r_i is given by $\overline{\delta}_i(r_i) + 1 = M/\bar{M}_i$. Using the energy integral, one finds $A_{\mathrm{sh}} = \frac{3}{10}\frac{r_i}{\delta(r_i)}$ and $B_{\mathrm{sh}} = \frac{1}{2H_0}(\frac{5}{3}\frac{\overline{\delta}_i(r_i)}{a_i})^{-\frac{3}{2}}$ (e.g., [62,69–71]).

Solutions for the Lagrangian radius r are self-similar, in the sense that r/r_i depends only on the development angle θ for any initial radius r_i at t_i, but θ_i is different for each shell. In accordance with the discussion of the previous subsection, we need these (no shell crossing) solutions to be valid at least until all shells have achieved maximal

expansion and turned around. In a realistic initial profile, with density decreasing with radius, shell crossing will first occur at the inner shells. To eliminate such crossing (including the innermost shell crossing itself before reexpanding) until all shells have turned around, one may thus require that $\theta(r_i = 0) \leq 2\pi$, when the outermost shell, initially at radius R_i, is turning around; i.e., when $\theta(R_i) = \pi$. In general, from the second of Eqs. (19), a shell initially at dimensionless radius $x = r_i/R_i$ will have a development angle

$$\theta_t(r_i) - \sin \theta_t(r_i) = \pi \left[\frac{\bar{\delta}_i(x)}{\bar{\delta}_i(R_i)} \right]^{3/2} \qquad (20)$$

at the turnaround of the outer shell. This implies that the maximum density contrast allowed between the initial central and average density is $[\frac{\delta_i(0)}{\delta_i(R_i)}]_{max} = 2^{2/3}$.

The overdensity within the maximal initial radius R_i can be assumed to correspond to the rms dispersion in the linear density field $\sigma_M(R_i, t_i)$. To complete the model, we then need a profile for the initial overdensity, in order to determine $\bar{\delta}_i(r_i)$. We follow [71] in using a simple generic density profile, with steepness adjusted through a parameter β,

$$\frac{\bar{\delta}_i(x)}{\bar{\delta}_i(R_i)} = \frac{\delta_i(0)}{\delta_i(R_i)}(1 - cx^\beta). \qquad (21)$$

The corresponding local (as opposed to volume averaged) density distribution has the same form but with $c \to c(\beta + 3)/3$. Figure 1 in [71] shows the profiles for various values of β (their Fig. 3 also shows the much steeper forms of these density contrast, when evolved until the turnaround of the outer shell). Here we will use three values of β, reflecting qualitatively different behaviors: $\beta = 7$, corresponding to nearly flat profile in the inner regions and steep decrease in outer ($x \gtrsim 0.5$) ones; $\beta = 1$, with density decreasing linearly with x; and $\beta = 0.1$, which corresponds to nearly flat profile in the outer region with rapid increase at small radii. Realistic initial peak profiles, obtained by smoothing the linear random field, are consistent with such a flat distribution at large radii, with steeper increase in the central region, as Fig. 10 of [71] illustrates. It also suggests that, for small mass halos collapsing at higher redshifts, which is our prime interest here, our relatively small initial maximal average overdensity contrast, chosen to ensure that no shell crossing occurs, is not unrealistic.

Assuming this maximal average density contrast fixes the first factor on the right-hand side of (21). Requiring $\frac{\bar{\delta}_i(x=1)}{\bar{\delta}_i(R_i)} = 1$, fixes c to $c = 1 - [\frac{\delta_i(0)}{\delta_i(R_i)}]^{-1}$. As noted, the average overdensity $\bar{\delta}_i(R_i)$ may be presumed to correspond to the linear $\sigma_M(R_i, z_i)$. To ensure such a correspondence— that overdensities are adequately linear at all radii $r_i(z_i)$

within the sphere—we start our evolution at $z_i = 300$ (larger than the starting redshift in the previous section). Given β, this fixes the profile completely.

The magnitudes of the pressure and gravitational forces are given by

$$|\boldsymbol{\nabla}\phi| = \frac{GM}{r^2}, \qquad (22)$$

$$\left| \frac{\boldsymbol{\nabla}P}{\rho} \right| = \frac{1}{\rho} \frac{dP}{d\rho} \frac{d\rho}{dr} = \frac{Ac^2}{\rho} \frac{d\rho}{dr_{ta}}, \qquad (23)$$

where we have assumed $\alpha = 1$ in Eq. (1), as for a fiducial Chaplygin fluid configuration. If the pressure forces are negligible along an evolution described by (19), the mass inside each shell is practically conserved and

$$M = M(< r_i) = 4\pi \int_0^{r_i} r^2 \rho_i dr, \qquad (24)$$

which is readily evaluated given (21). The local density is then given by

$$\rho = \frac{1}{4\pi r^2} \frac{dM}{dr}. \qquad (25)$$

With negligible pressure (and no shell crossing), $M = M(< r) = M(< r_i)$, and the density will depend only on the evolution of the Lagrangian coordinate r and its first derivative with respect to the initial condition r_i or, equivalently, on the change of volume between shells, as we detail in Appendix A, where we derive the pressure force along the unperturbed (gravity dominated) solution (19).

Our approach will be to assume the unperturbed solution (19), calculate the pressure and gravity forces along it as described, and contend the scheme to be self-consistent if we find $|\frac{\boldsymbol{\nabla}P}{\rho}|/|\boldsymbol{\nabla}\phi| \ll 1$ for all (r, t) or, equivalently, (r_i, θ), prior to shell crossing. In this case, the solution should hold to a good approximation, allowing for collapse into self-gravitating halos.

3. Conditions at turnaround and the nonlinear collapse scale

As noted in Sec. III B 1, the magnitudes of the gravitational forces driving the collapse are minimal at turnaround, while the competing pressure forces, hindering the collapse, are expected to be maximal near turnaround, as the average density inside a shell is minimal there. As these latter forces are determined by the local (as opposed to average) density and gradient, this statement can only be of approximate validity. However, the calculations of Appendix A show that this is generally a good approximation. We will therefore display our results here at turnaround, relegating the full evolution plots to the Appendix, while contending that $|\frac{\boldsymbol{\nabla}P}{\rho}|/|\boldsymbol{\nabla}\phi| \ll 1$ at turnaround points to the
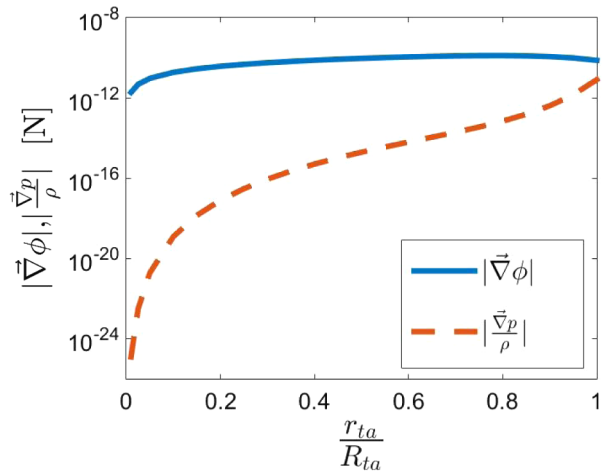
FIG. 7. Gravitational and pressure forces at turnaround for initial density profiles given by (21), with $\beta = 7$ (which is flat near the center and steeply decreasing for $x \gtrsim 0.5$) and $R_i = 1$ kpc (comoving). The system is started at $z = 300$ and evolved using (19), with initial average overdensity inside R_i corresponding to the rms fluctuation in the linear field $\sigma_M(1 \text{ kpc})$. The scaled radius on the x axis denotes the radius of turnaround of a certain shell relative to the radius of turnaround of the outer shell. As there is no shell crossing up to turnaround of all shells, smaller radii correspond to initially smaller $x = r_i/R_i$.

possibility of self-gravitating collapse and clustering in fiducial cosmological Chaplygin gas.

Figure 7 shows the results when the initial conditions correspond to the profile in (21) with $\beta = 7$, with an overdensity with boundary $R_i = 1$ kpc (comoving). As is clear, the gravitational force is dominant at turnaround for

all shells (at least by about an order of magnitude). We thus conclude that self-gravitating collapse is possible in this case. Figure 8 shows the situation when $\beta = 1$ or $\beta = 0.1$. These values correspond to profiles with initial density gradients that are less steep, when $x \gtrsim 0.5$, than in the former case; for $\beta = 1$ the density falls linearly with radius, while for $\beta = 0.1$ it is nearly flat except in the central region. As can be seen from the figure, the gravitational force is largely unaffected by the change in profile. However, the pressure forces are smaller in regions where the initial profiles have larger density or smaller gradient. And, again, these forces are invariably far smaller in magnitude than the gravitational ones, thus allowing for self-gravitating collapse.

Figure 9 shows the ratio of the magnitudes of the pressure to gravitational forces when the initial perturbation radii R_i correspond to the various indicated spatial scales. It shows that, at smaller scales, the pressure forces can become large enough to impede collapse, but that they gradually diminish relative to the gravitational force as the scale increases. The transition to a regime where they may be considered negligible generally occurs at an initial (comoving) perturbation scale of order 1 kpc. Thus, while the results of Sec. II D (particularly, Fig. 4), show that all the scales should be Jeans stable in the linear regime, one may now define a nonlinear Jeans scale at the kiloparsec scale. This phenomenon, absent in regular gases, arises from the peculiar property connected to the gas at hand, namely, the decreasing magnitude of the pressure with density.

From these results, it is clear that the collapse of comoving smoothing scales of $R \approx 100$ kpc, corresponding
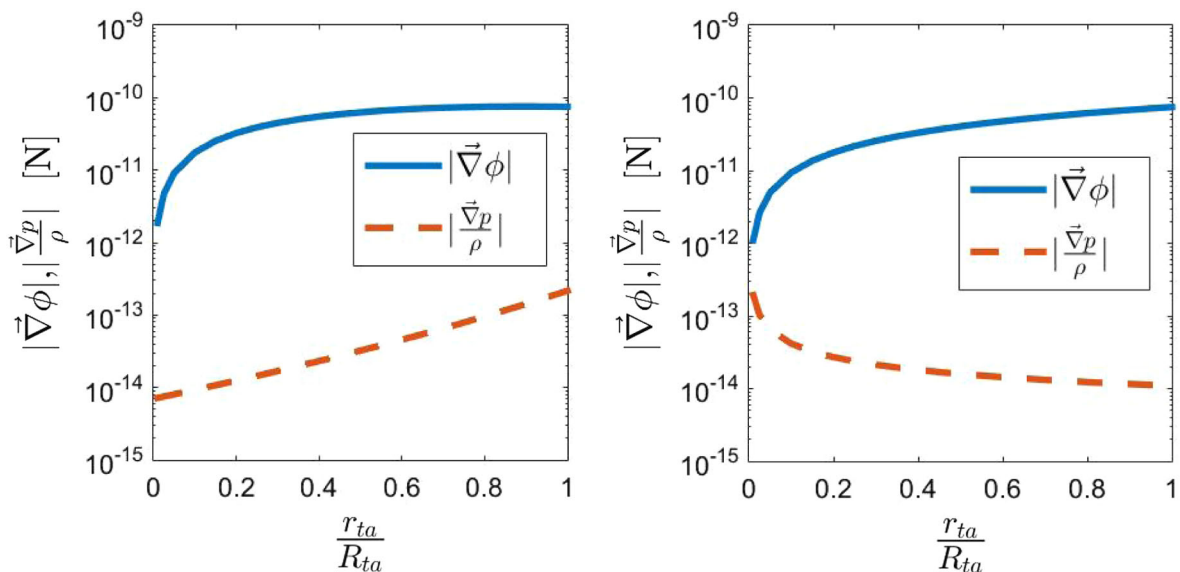

FIG. 8. Same as in Fig. 7, but for $\beta = 1$ (left) and $\beta = 0.1$ (right). The difference from the aforementioned figure reflects situations whereby the initial profile is linearly decreasing with radius ($\beta = 1$) or approximately flat except near the center ($\beta = 0.1$). The initial density gradients are smaller than for $\beta = 7$ in the outer regions.
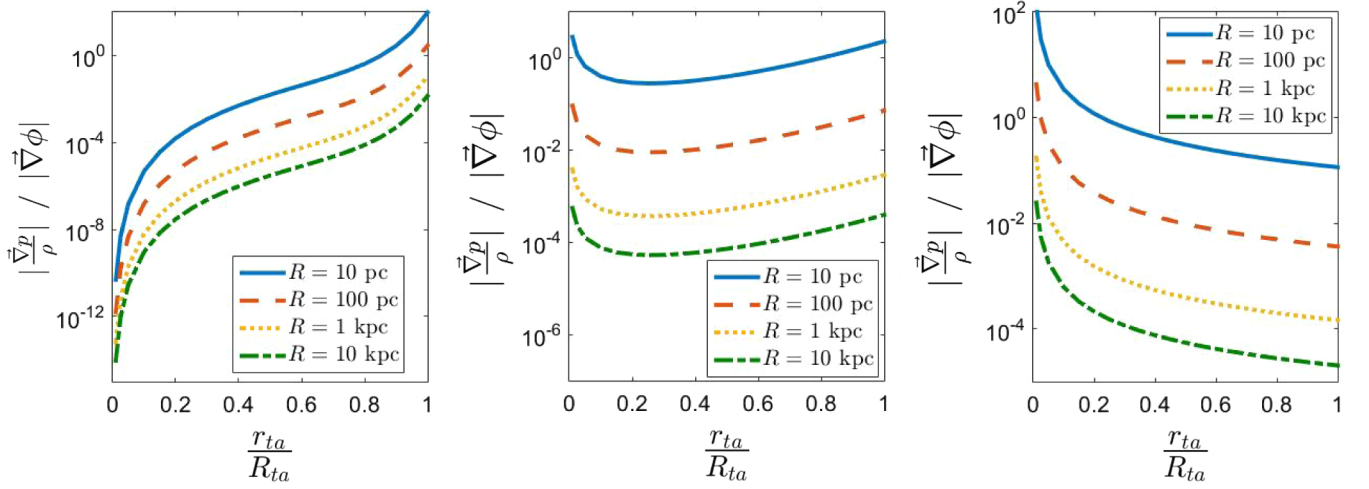
FIG. 9.   The ratio between the pressure to gravitational forces at turnaround for the profiles in (21), with $\beta = 7$, 1, and 0.1 (from left to right). The perturbations are probed at the various scales indicated. The transition scale at which the ratios switch from values smaller to ones larger than unity (at $R \approx 1$ kpc) constitutes what we have termed the nonlinear Jeans scale.

to halo masses of order $10^8 \, M_\odot$, may be readily realized as in CDM. This is likely to be the smallest halo mass scale relevant to observed dwarf satellite galaxies [72]. On the other hand, interestingly, significantly smaller scales would be progressively suppressed, which may be of relevance to the small scale problems associated with CDM [4,5].

IV. BACKREACTION ON BACKGROUND DYNAMICS

A. General considerations

The results of the previous section show that it is quite plausible for nonlinear clustering to occur in the standard Chaplygin gas. We here examine the effect of this phenomenon on the background evolution. As noted in [59], this may bring that evolution closer to that of the largely successful standard ΛCDM scenario. We illustrate this here in simplest terms, through modification of Eq. (3). For concreteness, we focus on the standard ($\alpha = 1$) case, though the results may be trivially generalized. We thus rewrite Eq. (3) as

$$\rho_{\mathrm{Ch}}(a) = \left(A_{\mathrm{cl}} + \frac{B_{\mathrm{cl}}}{a^6} \right)^{1/2}. \qquad (26)$$

As with A and B, the new coefficients A_{cl} and B_{cl} must be calibrated to be compatible with observations. At recombination ($a \sim 10^{-3}$), the first term in brackets is negligible (suppressed by a factor a^6 compared to the first).

In order to fit CMB data, with this component representing a matter contribution [73], one should have

$$B_{\mathrm{cl}} = B = \rho_m^2(a = 1) = \rho_c^2 \Omega_m^2. \qquad (27)$$

Then suppose that at $a = a_{\mathrm{cl}} < 10^{-1}$ the smallest scale that can cluster, in accordance with calculations of the previous

section, collapses into halos. A phase transition then occurs, with the clustered phase behaving thereafter as a pressureless component made of collapsed halos, which may henceforth hierarchically merge. We assume that a definite fraction of Chaplygin gas f splits into this CDM component. The density of the unclustered component then decreases by a factor $1 - f$, but unless the clustering is so efficient, such that $1 - f < 10^{-3}$, the first term in the bracket of (26) remains negligible. The density of the system then splits into

$$\rho = \rho_{\mathrm{Ch}} + \rho_{\mathrm{CDM}} = (1 - f) \frac{B^{1/2}}{a_{\mathrm{cl}}^3} + f \frac{B^{1/2}}{a_{\mathrm{cl}}^3}. \qquad (28)$$

For $f > 0.5$, most of the energy density is in the clustering component (with density ρ_{CDM}) at this point, while a minority remains in the form of homogeneous Chaplygin gas (with ρ_{Ch}). However, at late times (as $a \to 1$), the first term in Eq. (26) becomes important, and the total density (of homogeneous Chaplygin plus clustered CDM component) evolves as

$$\rho = \left(A_{\mathrm{cl}} + \frac{(1 - f)^2 B}{a^6} \right)^{1/2} + f \frac{B^{1/2}}{a^3}. \qquad (29)$$

Evaluating this at $a = 1$, and assuming a current critical density ρ_c, gives

$$A_{\mathrm{cl}} = A + 2f \rho_c^2 \Omega_m^2 \left(1 - \frac{1}{\Omega_m} \right), \qquad (30)$$

where $A = (1 - \Omega_m^2) \rho_c^2$ [from Eq. (4)].

For $f \to 0$, $A_{\mathrm{cl}} \to A$, as expected. It is worthwhile to note, however, that for $\Omega_m \approx 0.3$ and a high level of clustering, A_{cl} is significantly smaller than A. As a Chaplygin dark sector
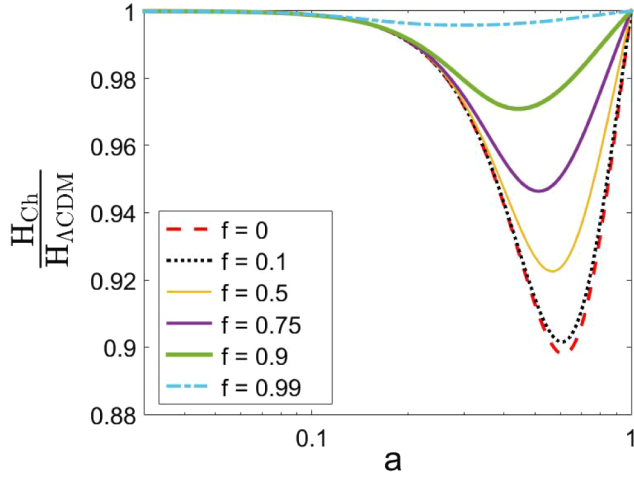
FIG. 10. Ratio of the evolution of the Hubble parameter in clustered standard Chaplygin gas universes [$\alpha = 1$ in Eq. (1)] to that of ΛCDM, with $\Omega_m = 0.3$ and $\Omega_\Lambda = 0.7$, for various values of the fraction f of the clustered (CDM) Chaplygin gas component.

that can support the observed large scale structure must embody a clustered medium, it would therefore be characterized by $A_{\rm cl}$, rather than A, in its equation of state. The calculations of the previous sections, where A was used as customary, thus involve larger sound speeds and pressure gradients. They should actually be considered conservative in estimating the relative strengths of the gravitational to pressure forces.

Because the terms suppressed by powers of a rapidly decrease with a, there are two transitions embodied in the form of Eq. (29). One occurs when $A_{\rm cl} \gtrsim \frac{B}{a^6}(1-f)^2$. This indicates that the nonclustered Chaplygin component has transited to a dark energy like fluid, behaving like a cosmological constant, with density $\rho_\Lambda = \sqrt{A_{\rm cl}}$. With $\Omega_m = 0.3$ and $f \to 1$, this nicely gives $\rho_\Lambda \to 0.7\rho_c$. This is not surprising, as the advent of a cosmological constant component renders the background evolution closer to ΛCDM than that of the homogeneous Chaplygin gas cosmology. We illustrate this in Fig. 10, where we plot the ratios of the Hubble parameter in flat clustered Chaplygin gas universes to those of ΛCDM, assuming the same values H_0 for all models at $z = 0$.

The transformation of the homogeneous component into a Λ-like sector occurs when

$$a_\Lambda \gtrsim \left(\frac{B}{A_{\rm cl}}\right)^{1/6}(1-f)^{1/3}, \qquad (31)$$

which happens at earlier a [by a factor $\sim(1-f)^{1/3}$], compared to the homogeneous Chaplygin gas scenario. The latter is still in transition at $a = 1$, causing tension with late Universe background cosmic dynamics [59].

Finally, we have the transition whereby the total cosmic energy density switches from being dark matter dominated to dark energy domination. By this time, the homogeneous Chaplygin component has already fully transited into its Λ-like phase. If we accordingly ignore the second term in Eq. (29), a clustered Chaplygin gas universe should transit to a dark energy dominated regime at $a \gtrsim f^{1/3}(\frac{B}{A_{\rm cl}})^{1/6}$. As the equation of state of the homogeneous dark energy component is now effectively that of a cosmological constant with $p = -\rho_\Lambda$, imposing the condition $\rho + 3p = 0$ leads to a deceleration-acceleration transition at

$$a_{\rm da} \gtrsim \left(\frac{f}{2}\right)^{1/3}\left(\frac{B}{A_{\rm cl}}\right)^{1/6}. \qquad (32)$$

With $\Omega_m = 0.3$ and $f \to 1$, this tends to $a_{\rm da} = 0.6$, with $z_{\rm da} = 0.67$, which is compatible with lower bounds inferred from observations. The transition redshift increases as f decreases. It remains within viable bounds $z_{\rm da} \lesssim 1$ as long as the clustering is efficient ($f \gtrsim 0.7$).

One can thus count three transitions. The first one leads to a clustered medium, whereby part of the Chaplygin gas collapses into halos and acts henceforth as a CDM-like component; the second transition occurs when the remaining homogeneous gas starts to effectively act as a cosmological constant; whereas the third transition takes place when the Chaplygin universe transits to an accelerated phase. This latter development occurs much the same way as Λ becomes dominant in the standard model. Furthermore, when the matter energy density is calibrated to the CMB, the Λ-like component comes with energy density compatible with its measured late time value in the context of the ΛCDM model. The basic characteristics of the clustered Chaplygin cosmology appear in this context quite akin to ΛCDM, including a similar transition time for its transformation from decelerated to accelerated expansion.

B. Constraints from observations

The general considerations just described suggest that the background evolution of clustered Chaplygin gas cosmologies may be viable, provided that the fraction that clusters into a CDM-like component (f) is large enough. In order to obtain specific quantitative constraints on f, we confront the model with observational datasets constraining the background cosmology. For this purpose, we use supernova SNe 1a, baryon acoustic oscillation (BAO), and CMB data, in addition to cosmic chronography (CC) estimates of the Hubble parameter $H(z)$.

For supernova data we use the Pantheon sample [74,75], combining data from the Pan-STARRS1 Medium Deep Survey with older observations, for a total 1048 SNe Ia in the redshift range $0.01 < z < 2.3$. We also use anisotropic BAO data from the Sloan Digital Sky Survey III, as provided in [76], to simultaneously constrain the Hubble

parameter and the angular diameter distance. Additional constraints on $H(z)$ come from CC data obtained from [77]. As the CMB spectrum at last scattering ($z = z_*$) is practically unaffected by the modification of late time dark energy behavior introduced by replacing ΛCDM by a Chaplygin gas dark sector (as the contribution to the total energy density from the dark energy component at z_* is of order $1/z_*^3 \lesssim 10^{-9}$ in both cases), constraints on the background evolution may be effectively expressed by a "compressed likelihood" of the CMB power spectrum [78,79]. This includes the shift parameter $\mathcal{R} = \frac{1}{c}D_M(z_*)\sqrt{\Omega_m H_0^2}$, where D_M is the comoving angular diameter distance to last scattering, which in a flat Friedmann-Robertson-Walker universe is given by

$$D_M(z_*) = c \int_0^{z_*} \frac{dz}{H(z)}. \tag{33}$$

Another CMB distance prior is the angular scale of the sound horizon at last scattering $l_A = \pi D_M(z_*)/r_s(z_*)$, where $r_s(z_*)$ is the comoving sound horizon at z_*. Finally, an additional constraint is obtained from the present physical baryon density $\omega_b = \Omega_b \rho_c$. We use the following values, based on an analysis of the Planck-2018 TT, TE, EE + lowE data [80]: $\mathcal{R} = 1.7502 \pm 0.0046$, $l_A = 301.471^{+0.089}_{-0.090}$, and $\Omega_b h^2 = 0.02236 \pm 0.00015$. We note the particularly strong constraint on l_A: $|\Delta l_A|/l_A \simeq 3 \times 10^{-4}$.

To enable proper comparison with those datasets, the equations of the previous subsection are modified, so as to account for separate baryonic and radiation components. Thus, B now refers just to the dark matter density, so that $B_{\rm cl} = B = \rho_c^2 \Omega_c^2 = \omega_c^2$, and Eq. (29) has two additional additive terms, incorporating the baryon and radiation energy densities, namely, Ω_b/a^3 and Ω_R/a^4. Also, by defining $\rho(a = 1) = \rho_c$, one now has

$$A_{\rm cl} = \rho_c^2[\Omega_{\rm Ch}^2 - (1 - f)^2 \Omega_c^2], \tag{34}$$

where $\Omega_{\rm Ch} = 1 - (f\Omega_c + \Omega_b + \Omega_R)$.

The modified Eq. (29) is then included into the publicly available code CLASS [81], in order to evaluate the theoretical predictions. The statistical analysis is conducted by running a Monte Carlo Markov chain (MCMC) over models, using the publicly available EMCEE code [82].

Keeping the number of relativistic degrees of freedom fixed as in standard cosmology, the background evolution of the clustered Chaplygin gas universe is determined by four parameters. Three of these (H_0, ω_b, and ω_c) are shared with ΛCDM, with which we will be comparing our clustered Chaplygin gas models, by conducting control MCMC runs. For these parameters, we take flat priors in the following forms: $H_0 = [65:80]$ km/s/Mpc, $\Omega_c h^2 = [0.1:0.131]$ and $\Omega_b h^2 = [0.015:0.028]$. A prior is also placed on the absolute magnitudes of the SNe Ia: $M = [-20:-18]$.

The additional parameter in our clustered Chaplygin model is the clustering fraction f. When $f \to 0$, one recovers the conventional Chaplygin gas, which has been shown to be strongly disfavored by observations [recall that we are assuming, throughout this section, that we are dealing with a standard Chaplygin gas with $\alpha = 1$ in Eq. (1)]. Here we want to examine the likelihood of clustered models characterized by different f. For this purpose, we place a flat prior encompassing the whole range of possibilities $f = [0:1]$. The posterior probabilities of all parameters are then obtained from the MCMC analysis.

The results are shown in Fig. 11. The best fit values for the clustered Chaplygin gas is $f \simeq 0.95$. Values down to $f = 0.91$ are allowed at the 1-sigma level. Slightly smaller values of $f \gtrsim 0.88$ are allowed at 2-sigma. The background
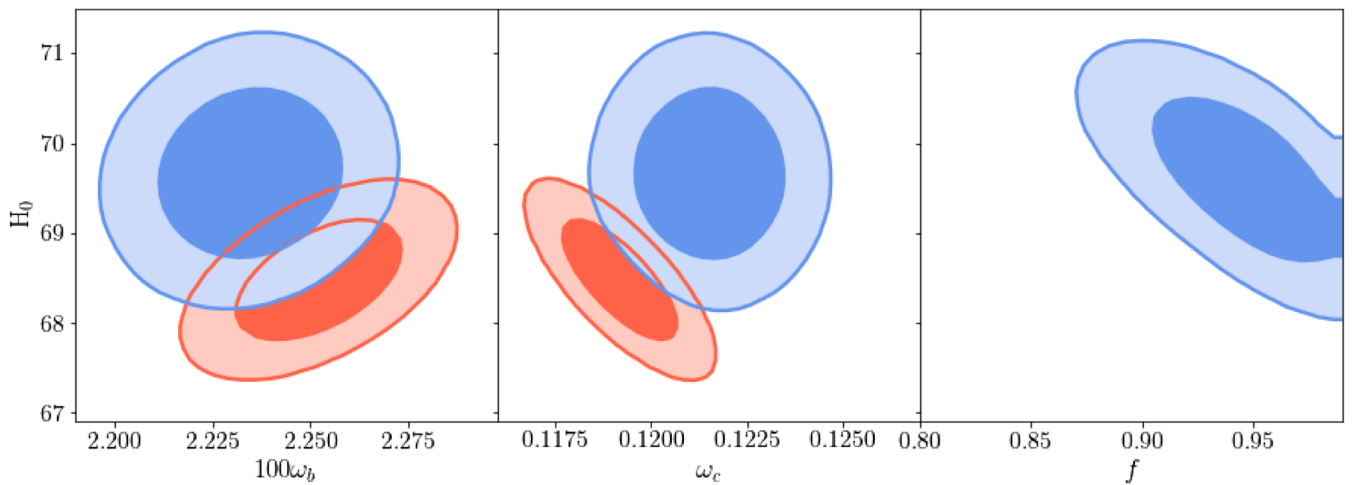

FIG. 11. 1- and 2-sigma contours of the Hubble parameter and physical baryon and dark matter densities at $z = 0$, in flat clustered Chaplygin gas universes (blue) and ΛCDM (red). In the former case, we also show the distribution of the clustering fraction f against H_0. The dataset used includes SNe Ia, CMB, and BAO data, as well as CC estimates of $H(z)$. The χ^2 for the best fitting ΛCDM and Chaplygin models are 1054 and 1048, respectively (with corresponding reduced χ^2/dof of 1.027 and 1.021).
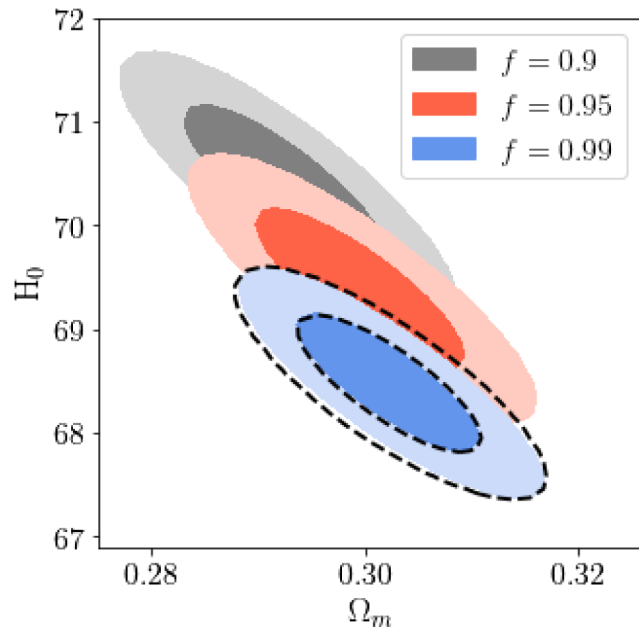
FIG. 12. Convergence of clustered Chaplygin models toward ΛCDM as the clustered fraction $f \to 1$. Dashed contours refer to ΛCDM. Note the systematically larger H_0 for smaller f.
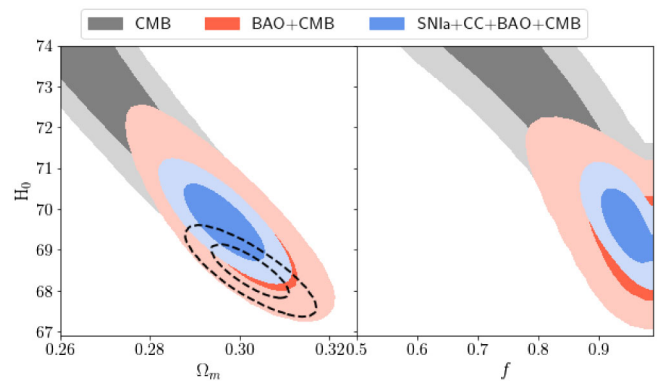

FIG. 13. Constraints from the various datasets. While ΛCDM is highly constrained by CMB data, clustered Chaplygin gas models are compatible with larger H_0 if the clustered fraction f is relatively small. Smaller values of f (and larger H_0) are, however, disfavored by other datasets (primarily by high precision intermediate distance measurements coming from the BAO). Thus, favored models remain close to ΛCDM (represented by the dashed contours).

evolution of the clustered Chaplygin gas may thus be considered viable for these clustering levels and associated levels of confidence. Indeed, we find the total χ^2 is slightly smaller for the best fitting clustered Chaplygin gas than the best fitting ΛCDM (1054 versus 1048). On the other hand, the unclustered standard Chaplygin gas model, with $f \to 0$ (and $\alpha = 1$), is clearly ruled out, as expected. At the opposite limit, as $f \to 1$, the model tends toward ΛCDM, as expected from the discussion of the previous subsection and as illustrated in Fig. 12.

The mean value of H_0 for the clustered Chaplygin models is larger than that obtained for ΛCDM, namely, 69.7 km/s/Mpc for the former versus 68.5 km/s/Mpc for the latter, when f is left free. When f is fixed, H_0 is also systematically higher for smaller f (Fig. 12).

The larger H_0 in the Chaplygin case can be understood in terms of the behavior of the Hubble parameter shown in Fig. 10, noting again that the acoustic scale l_A is the most strongly constrained observable in our analysis. This principally translates into a constraint on the comoving angular diameter distance to the CMB last scattering surface. In ΛCDM this distance is entirely fixed, given the physical energy densities associated with radiation, dark matter, baryons, and the cosmological constant. However, since (from Fig. 10), when $H_{\mathrm{Ch}}/H_{\Lambda\mathrm{CDM}}$ is set to unity at $z = 0$, for $z > 0$ and $f < 1$ there are intervals for which the ratio is smaller than unity, it follows from Eq. (33) that one can obtain the same value for D_M by rescaling $H_{\mathrm{Ch}}(z)$, such that $H_{\mathrm{Ch}}(z = 0)/H_{\Lambda\mathrm{CDM}}(0) > 1$. The effect is illustrated in Fig. 13 in terms of the likelihood contours.

This situation is similar to the case of phantom dark energy models. And, as in that case, one may actually entirely "solve" the H_0 tension, if this is solely defined as a tension between local and CMB measurements of H_0. However, also as in the phantom case, distance measures on the way to the CMB, particularly high precision BAO data, constrain the models to be close to ΛCDM [83]. In the present context, this requires f to be close to unity and thus H_0 to be only slightly larger than in ΛCDM, compared to what is needed to entirely alleviate the H_0 tension. The behavior of the ratio of $H(z)$ for the best fitting Chaplygin and ΛCDM models, reflecting the competing constraints, is shown in the lower panel of Fig. 14.
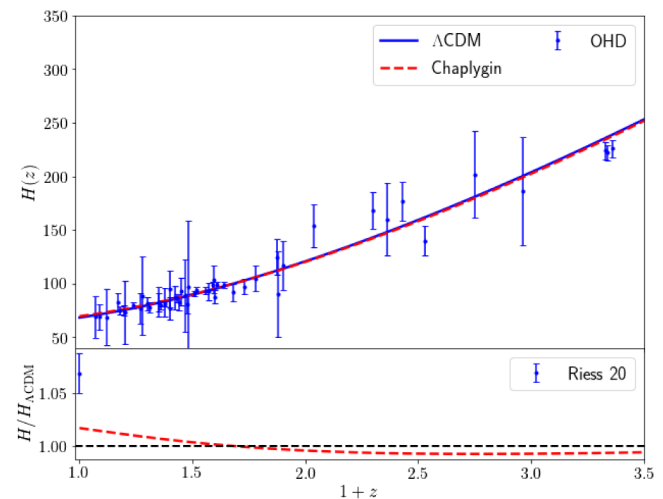

FIG. 14. Observational Hubble data (OHD), from CC and BAO measurements, and best fitting ΛCDM and clustered Chaplygin models. The local value of H_0, as measured by Riess *et al.* [84], is also shown in the lower panel (but not included in the likelihood analysis of either model).

V. CONCLUSION

Unified dark matter models are appealing for combining the dark sector in a single component, which can act as both dark energy and dark matter. The prototypical example is that of the generalized Chaplygin gas, with equation of state (1), providing for small pressure at high densities and significant negative pressure at low density. However, unless the generalized Chaplygin gas parameter is chosen such that the associated cosmology is virtually indistinguishable from ΛCDM, or superluminal sound speeds are allowed, linear perturbations in a homogeneous Chaplygin fluid will become Jeans stable and oscillate acoustically and damp, rather than grow, on scales observed in large scale structure surveys. This, in particular, is true for the theoretically motivated standard Chaplygin gas with $\alpha = 1$.

Here we first note that, in a hierarchical structure formation model, dark matter perturbations probed by large scale structure surveys do not occur in a homogeneous fluid. Rather, they occur in a medium that is already hierarchically clustered, starting from dwarf galaxy scales or smaller. It is sufficient for the Chaplygin fluid to collapse into halos early on, on some small scale (dwarf galaxy halo or below), for a CDM-like component to materialize and cluster hierarchically.

We thus ask whether any small scale seed perturbations can grow sufficiently to collapse early on. We first examine the linear stability and check whether perturbations may grow to reach the usual Press-Schechter threshold required for nonlinear collapse. We find that, while this may be the case for very small or large values of α, such an analysis suggests that acoustic oscillations generally prevent the achievement of the threshold. However, for the fiducial case of $\alpha = 1$, the rms fluctuations do come quite close to achieving the critical threshold for scales associated with dwarf galaxies and below.

That the perturbations come tantalizingly close to crossing the critical collapse threshold for this relatively well motivated model—and at the minimal scales expected in a successful hierarchical collapse model, with no free parameters tuned—suggests that a nonlinear analysis is warranted. This is particularly motivated by the fact that pressure forces in a unified dark matter fluid decrease in magnitude with increasing density (characteristic of nonlinear phase), as opposed to the case of laboratory fluids where the pressure and its gradients become more important as the density increases. Thus, systems that are stable against self-gravitating collapse in the linear regime may not be so in a nonlinear analysis.

Numerical and theoretical modeling of the dynamics of a negative pressure fluid with sound speed decreasing with density is largely unexplored. Through a simple secondary infall model, we attempt to circumvent expected difficulties, while capturing the basic ingredients that determine the possibility of collapse and formation of self-gravitating objects in the nonlinear regime. We choose the initial density distribution to correspond to a system where all shells turn around, before any shell crossing occurs, when the system is evolved solely under gravity. Then we evolve the dynamics, starting in the linear regime at high redshift. We show that while a linear analysis predicted that kiloparsec scale perturbations were marginally (Jeans) stable, nonlinear evolution suggests that pressure forces should, in fact, be negligible compared to gravitational ones along the whole inhomogeneous top hat trajectory, for perturbations on scales $\gtrsim 1$ kpc, thus enabling gravitating collapse.

One may, in this context, define a nonlinear Jeans scale, which does not have a counterpart in standard gases. It arises from the peculiar characteristic of the decreasing magnitude of the pressure in Chaplygin gases. Nonlinear perturbations larger than this Jeans length can also grow, as the ratio of the gravitational forces becomes smaller still. In particular, the collapse of comoving scales associated with small dwarf satellite galaxies should be readily allowed.

Once structures form on small scales, a CDM-like component is present. It may proceed to cluster hierarchically, independent of the remaining homogeneous Chaplygin fluid. The latter may still act as dark energy. The acoustic oscillations, thought to rule out unified dark fluid models, would only be imprinted in that dark energy component and would not appear in the galaxy power spectrum, which would correspond to CDM.

The formation of structure on scales smaller than the nonlinear Jeans scale, on the other hand, would be suppressed. This may be of relevance to the small scale problems associated with CDM, for example, the apparent overabundance of small CDM halos compared to the number of small galaxies observed. As with particle CDM alternatives, devised in part to address such problems, a Chaplygin gas model may be tested with observations of small scale structure [85,86].

In light of these results, the problem of acoustic oscillations in the linear power spectrum of Chaplygin gases may not be as serious as usually assumed, provided the hierarchical structure formation process is adequately taken into account. In particular, it would appear less serious than the problem of finding self-gravitating equilibrium with a density distribution corresponding to that inferred from observations at large radii around galaxies and clusters, while keeping the same equation of state [87].

Furthermore, in the context of the present analysis, the basic characteristic background evolution of the clustered Chaplygin gas cosmology is found to tend toward ΛCDM as the clustering efficiency is increased: when clustering occurs, the remaining homogeneous component constitutes a cosmological constant sector early on, with an energy density akin to the corresponding one in ΛCDM; the acceleration deceleration transition occurs also as in the standard models. Finally, the pressure forces associated with the clustered gas are smaller [through a rescaling of the parameter A in Eq. (1), as described in Sec. IV]. This

reinforces the consistency of the collapse model and may also help alleviate the aforementioned problems related to the dynamics of the outer parts of galaxies and clusters.

Quantitative comparison with observational datasets shows the background dynamics of the clustered Chaplygin gas models to be viable (at the 1-sigma level) if the fraction of fluid that collapses into a CDM-like component of small halos (that may subsequently hierarchically cluster) is larger than 90%. The associated value of the Hubble constant is larger than in ΛCDM, due to effects similar to those present in phantom dark energy models. As in these models, the "Hubble tension" may be completely resolved if it is defined solely in terms of discrepancy between local and CMB measurements. However, other data, particularly high accuracy BAO distance measurements, dictate that viable models (and their H_0) remain relatively close to ΛCDM.

Further investigation, beyond the simple nonlinear collapse model presented here, requires an examination of what happens at shell crossing in the later stages of self-gravitating collapse, including the treatment of possible shocks. Though some work regarding the Riemann problem for Chaplygin gas exists in the mathematical literature, including idealized shock simulations [66–68], the physical consequences of the phenomenon remains unexplored. To our knowledge, no detailed numerical simulations of the dynamics of any Chaplygin fluids have been conducted, much less of its self-gravitating cosmological evolution. We hope that the proof of principle presented here, suggesting that the problem of large scale oscillations in the power spectrum should not be as insurmountable as widely believed, would help reopen detailed investigation of the consequences of structure formation in the context of Chaplygin gas cosmologies.

APPENDIX A: RATIO OF PRESSURE TO GRAVITY FORCE ALONG PARAMETRIC SOLUTION

We wish to evaluate the relative magnitude of the gravity to pressure forces along the cycloid solution (19). As this solution reflects evolution solely under the influence of gravity (and with no shell crossing), it would still approximately hold if the pressure forces remain small relative to gravity along it, at all temporal stages and spatial radii.

Before shell crossing occurs, finding the gravitational force on a shell at radius r is trivial; it is simply given by $-GM/r^2$, with the mass M enclosed in r taken as constant, and the radius given by the first by the cycloid solution (19). To evaluate the pressure forces along this "unperturbed" solution, we map the evolution of the local density and its gradient along it. For this purpose, we consider neighboring initial conditions, starting at same initial time $t = t_i$ and developing according to Eqs. (19).

In the absence of shell crossing, the evolving density $\rho(r, t)$ is given in terms of the initial distribution ρ_i through
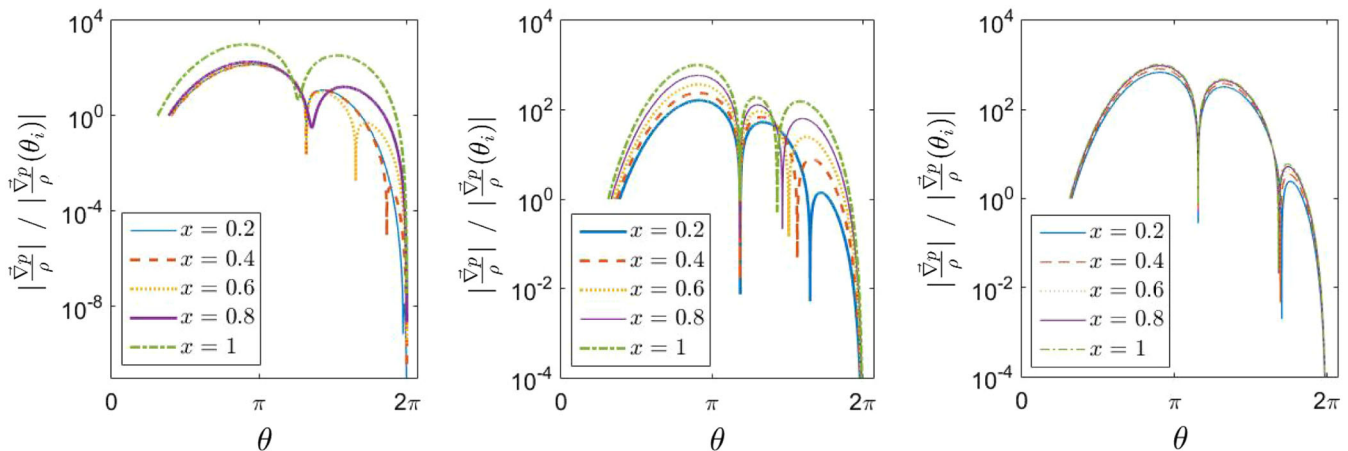

FIG. 15. Scaled pressure along parametric solution (19) at various values of the scaled initial radius $x = r_i/R_i$. The initial density profiles are given by (21) with (from left to right) $\beta = 7$, 1, and 0.1 and $R_i = 1$ kpc, starting at $z_i = 300$ with overdensity equal to the rms fluctuation of the linear Gaussian field: $\bar{\delta}(R_i) = \sigma_M(R_i, z_i)$. The derivative discontinuities (reflecting sign switching in d^2r/dr_i^2 and dr/dr_i) correspond to consecutive shells approaching instead of increasing their separation and then to eventual shell crossing. The calculation of the pressure beyond this (shell crossing) point is only formal, as the dynamics reflected in the solution (19) no longer strictly apply. Note that the steeper the change in density through the bulk of the system (larger β), the more spaced out the discontinuity angles for different values of x.
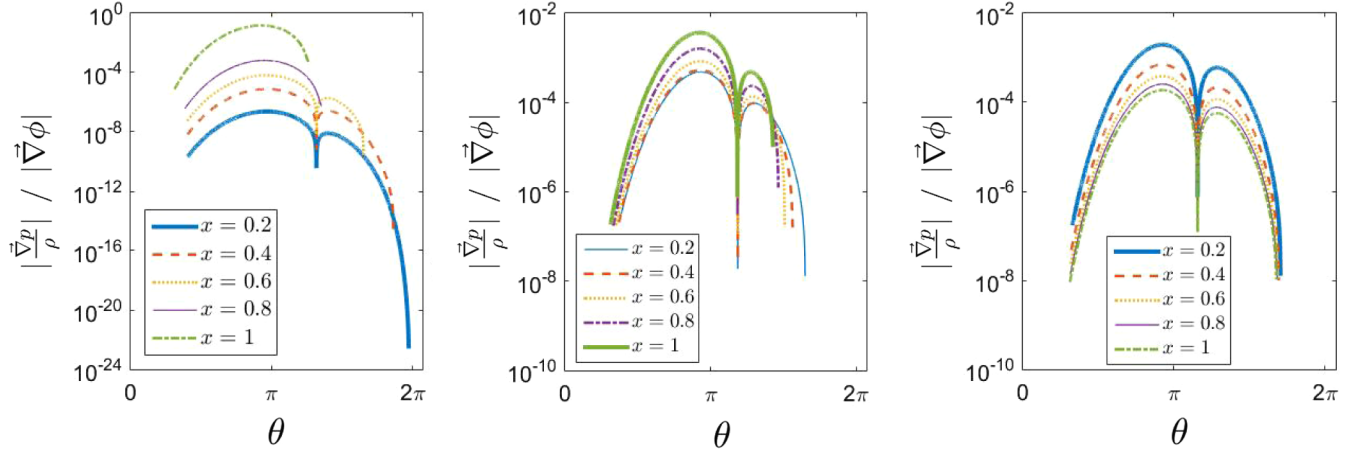
FIG. 16. Same as in Fig. 15, but for the ratio of pressure to gravitational force and until local shell crossing occurs.

the change of the volume element between neighboring shells. Namely,

$$\rho(r,t) = \left|\frac{dV_i}{dV}\right| \rho_i(r_i, t_i), \tag{A1}$$

where [using the first of Eqs. (19)]

$$\left|\frac{dV_i}{dV}\right| = \frac{r_i^2}{r^2}\left|\frac{dr_i}{dr}\right| = \left(\frac{1-\cos\theta_i}{1-\cos\theta}\right)^2\left|\frac{dr_i}{dr}\right|. \tag{A2}$$

The density gradient can also be written as

$$\frac{d\rho(r,t)}{dr} = \frac{dr_i}{dr}\left(\left|\frac{dV_i}{dV}\right|\frac{d\rho_i(r_i,t_i)}{dr_i} + \rho_i(r_i,t_i)\frac{d}{dr_i}\left|\frac{dV_i}{dV}\right|\right). \tag{A3}$$

The explicit forms of the terms required to calculate the density and its gradient for the profiles adopted in this study are given in Appendix B. We here present the results. As in the main text, we use the code CAMB to produce $\sigma_M(R_i)$ at $z_i = 300$, with $H_0 = 69 \text{ km s}^{-1} \text{ Mpc}^{-1}$.

Figure 15 shows results for the scaled pressure forces on various shells are shown for the three chosen values of β, reflecting flatter initial outer profiles (i.e., as $x = r_i/R_i \to 1$) for the standard Chaplygin gas ($\alpha = 1$). As may be expected (and already noted in Sec. III B 2), given the equation of state (1), the pressure force increases as a shell expands, reaching a maximum near turnaround. It then rapidly decreases as the shell contracts. The derivative discontinuities correspond to switching in signs in the second derivatives of the radial coordinate with respect to the initial conditions—signaling that shells are approaching rather than increasing their separation—and then in the first derivatives, when shell crossing eventually occurs. This occurs with wider spacing for steeper initial density gradients because, in the limit of homogeneous monolithic collapse, shell crossing occurs for all shells at the same θ

(and θ_i is also the same for all shells, as opposed to the case here).

Beyond shell crossing, our model no longer strictly applies. The model also becomes inconsistent if the pressure forces—at any $\theta \leq \pi$, for any shell—become comparable to the gravitational forces; in this case, the gravitationally dominated dynamics of the unperturbed trajectories are no longer a good approximation. As Fig. 16 shows, however, this is not the case. Although, before turnaround ($\theta = \pi$), the pressure force systematically increases and the gravity decreases, as the system expands, the ratio remains much smaller than unity, for all shells and all models. The maximum value of the ratio is reached at turnaround. Beyond turnaround, the increasing density (hence generally decreasing pressure) and increasing gravity ensures that the pressure forces become smaller still relative to the gravitational ones. This renders self-gravitating collapse possible. As discussed in Sec. III B 3 (particularly in relation to Fig. 9) this conclusion is strengthened for larger scale nonlinear perturbations. The collapse of comoving smoothing scales corresponding to a halo mass scale relevant to dwarf galaxies should be readily allowed. On the other hand, structure formation on significantly smaller scales would be progressively suppressed, which would, in turn, be of relevance to the small scale problems associated with CDM structure formation.

APPENDIX B: EXPLICIT FORMS OF THE DENSITY AND ITS GRADIENT ALONG PARAMETRIC SOLUTION

To find $\left|\frac{dr_i}{dr}\right|$, we use the first of Eqs. (19), to obtain

$$\frac{dr}{dr_i} = \frac{dA_{\text{sh}}}{dr_i}(1 - \cos\theta) + A_{\text{sh}}\sin\theta\frac{d\theta}{dr_i}. \tag{B1}$$

This may be readily evaluated using $\frac{d\theta}{d\theta_i}\frac{d\theta_i}{dr_i}$, and noting that, as we are studying divergences between neighboring cells

at fixed time, the condition $dt = 0$ may be imposed on the second of Eqs. (19) to obtain

$$\frac{d\theta}{d\theta_i} = -\frac{\frac{dB_{\mathrm{sh}}}{d\theta_i}(\theta - \sin\theta)}{B_{\mathrm{sh}}(1 - \cos\theta)}. \tag{B2}$$

For the family of profiles given by (21), and assuming an initial overdensity corresponding to the rms fluctuations of the linear density field such that $\delta(\bar{R}_i) = \sigma_M(R_i)$ at the initial time t_i, one finds

$$\frac{d\theta_i}{dr_i} = \frac{\frac{10}{3}2^{2/3}\sigma_M c\beta(\frac{r_i}{R_i})^{\beta-1}}{R_i \sin\theta}. \tag{B3}$$

Also, as $A_{\mathrm{sh}} = \frac{3}{10}\frac{r_i}{\bar{\delta}(r_i)}$ and $B_{\mathrm{sh}} = \frac{1}{2H_0}(\frac{5}{3}\frac{\bar{\delta}(r_i)}{a_i})^{-3/2}$ (Sec. III B 2 and references therein), we have

$$\frac{dA_{\mathrm{sh}}}{dr_i} = \frac{3}{10\bar{\delta}(r_i)} + \frac{3}{10}\frac{2^{2/3}\sigma_M c\beta(\frac{r_i}{R_i})^{\beta}}{\bar{\delta}(r_i)^2}, \tag{B4}$$

$$\frac{dB_{\mathrm{sh}}}{d\theta_i} = -\frac{3\sin\theta_i}{8H_0 a_i}\left(\frac{5\bar{\delta}(r_i)}{3a_i}\right)^{-5/2}. \tag{B5}$$

The density evolution of the density of these profiles can then be evaluated along the parametric solution using Eqs. (A1) and (A2).

In order to obtain the density gradient, we need to evaluate $\frac{d}{dr_i}|\frac{dV_i}{dV}|$. From (A2), this first requires obtaining

$$\frac{d}{dr_i}\left(\frac{r_i^2}{r^2}\right) = \frac{200}{9}\frac{\bar{\delta}(r_i)}{(1-\cos\theta)^2}\frac{d\bar{\delta}(r_i)}{dr_i} - \frac{200}{9}\bar{\delta}(r_i)^2\frac{\sin\theta}{(1-\cos\theta)^3}\frac{d\theta}{dr_i}, \tag{B6}$$

in addition to

$$\frac{d}{dr_i}\left|\frac{dr_i}{dr}\right| = -\left|\frac{dr}{dr_i}\right|^{-2}\frac{d}{dr_i}\left|\frac{dr}{dr_i}\right|. \tag{B7}$$

The first derivative appearing here is obtained as described above. For the second derivative, one has

$$\begin{aligned}\frac{d^2r}{dr_i^2} = &-\frac{3}{5\bar{\delta}(r_i)^2}\frac{d\bar{\delta}(r_i)}{dr_i}(1-\cos\theta) + \frac{3}{5\bar{\delta}(r_i)}\sin\theta\frac{d\theta}{dr_i}\\ &+\frac{3}{10}\frac{2r_i}{\bar{\delta}(r_i)^3}\left(\frac{d\bar{\delta}(r_i)}{dr_i}\right)^2(1-\cos\theta)\\ &-\frac{3}{10}\frac{r_i}{\bar{\delta}(r_i)^2}\frac{d^2\bar{\delta}(r_i)}{dr_i^2}(1-\cos\theta) - \frac{3}{5}\frac{r_i}{\bar{\delta}(r_i)^2}\frac{d\bar{\delta}(r_i)}{dr_i}\sin\theta\frac{d\theta}{dr_i}\\ &+\frac{3}{10}\frac{r_i}{\bar{\delta}(r_i)}\cos\theta\left(\frac{d\theta}{dr_i}\right)^2 + \frac{3}{10}\frac{r_i}{\bar{\delta}(r_i)}\sin\theta\frac{d^2\theta}{dr_i^2}.\end{aligned} \tag{B8}$$

Here,

$$\begin{aligned}\frac{d^2\theta}{dr_i^2} = &-\frac{10}{3}\frac{d\bar{\delta}(r_i)}{dr_i}\frac{\cos\theta_i}{\sin\theta_i^2}\frac{d\theta}{dr_i} + \frac{10}{3}\frac{d^2\bar{\delta}(r_i)}{dr_i^2}\frac{1}{\sin\theta_i}\frac{d\theta}{d\theta_i}\\ &+\frac{9}{20}\frac{\cos\theta_i}{\bar{\delta}(r_i)}\frac{\theta-\sin\theta}{1-\cos\theta}\left(\frac{d\theta_i}{dr_i}\right)^2\\ &-\frac{9}{20}\frac{1}{\bar{\delta}(r_i)^2}\frac{d\bar{\delta}(r_i)}{dr_i}\sin\theta_i\frac{\theta-\sin\theta}{1-\cos\theta}\frac{d\theta_i}{dr_i} + \frac{9}{20}\frac{\sin\theta_i}{\bar{\delta}(r_i)}\frac{d\theta}{dr_i}\frac{d\theta_i}{dr_i}\\ &-\frac{9}{20}\frac{\sin\theta_i}{\bar{\delta}(r_i)}\frac{\sin\theta(\theta-\sin\theta)}{(1-\cos\theta)^2}\frac{d\theta}{dr_i}\frac{d\theta_i}{dr_i}.\end{aligned} \tag{B9}$$

For the profiles (21),

$$\frac{d\bar{\delta}(r_i)}{dr_i} = -\sigma_M 2^{2/3}c\beta\frac{1}{R_i}\left(\frac{r_i}{R_i}\right)^{\beta-1} \tag{B10}$$

and

$$\frac{d^2\bar{\delta}(r_i)}{dr_i^2} = -\sigma_M 2^{2/3}c\frac{\beta(\beta-1)}{R_i^2}\left(\frac{r_i}{R_i}\right)^{\beta-2}. \tag{B11}$$

[1] C. S. Frenk and S. D. White, Dark matter and cosmic structure, Ann. Phys. (Berlin) **524**, 507 (2012).

[2] J. R. Primack, Triumphs and tribulations of ΛCDM, the double dark theory, Ann. Phys. (Berlin) **524**, 535 (2012).

[3] E. Di Valentino, O. Mena, S. Pan, L. Visinelli, W. Yang, A. Melchiorri, D. F. Mota, A. G. Riess, and J. Silk, In the realm of the Hubble tension − a review of solutions, Classical Quantum Gravity **38**, 153001 (2021).

[4] A. Del Popolo and M. Le Delliou, Small scale problems of the ΛCDM model: A short review, Galaxies **5**, 17 (2017).

[5] J. S. Bullock and M. Boylan-Kolchin, Small-scale challenges to the ΛCDM paradigm, Annu. Rev. Astron. Astrophys. **55**, 343 (2017).

[6] P. Salucci, The distribution of dark matter in galaxies, Astron. Astrophys. Rev. **27**, 2 (2019).

[7] G. De Rosa et al., Black hole mass estimates and emission-line properties of a sample of redshift $z > 6.5$ quasars, Astrophys. J. **790**, 145 (2014).

[8] X.-B. Wu, F. Wang, X. Fan, W. Yi, W. Zuo, F. Bian, L. Jiang, I. D. McGreer, R. Wang, J. Yang, Q. Yang,

D. Thompson, and Y. Beletsky, An ultraluminous quasar with a twelve-billion-solar-mass black hole at redshift 6.30, Nature (London) **518,** 512 (2015).

[9] D. Watson, L. Christensen, K. K. Knudsen, J. Richard, A. Gallazzi, and M. J. Michałowski, A dusty, normal galaxy in the epoch of reionization, Nature (London) **519,** 327 (2015).

[10] C. L. Steinhardt, P. Capak, D. Masters, and J. S. Speagle, The impossibly early galaxy problem, Astrophys. J. **824,** 21 (2016).

[11] R. Valiante, R. Schneider, M. Volonteri, and K. Omukai, From the first stars to the first black holes, Mon. Not. R. Astron. Soc. **457,** 3356 (2016).

[12] M. Stefanon, R. J. Bouwens, I. Labbé, A. Muzzin, D. Marchesini, P. Oesch, and V. Gonzalez, The rest-frame optical (900 nm) galaxy luminosity function at $z \sim 4$–7: Abundance matching points to limited evolution in the M_{STAR}/M_{HALO} ratio at $z \geq 4$, Astrophys. J. **843,** 36 (2017).

[13] K. Glazebrook, C. Schreiber, I. Labbé, T. Nanayakkara, G. G. Kacprzak, P. A. Oesch, C. Papovich, L. R. Spitler, C. M. S. Straatman, K.-V. H. Tran, and T. Yuan, A massive, quiescent galaxy at a redshift of 3.717, Nature (London) **544,** 71 (2017).

[14] B. P. Venemans, F. Walter, R. Decarli, E. Bañados, C. Carilli, J. M. Winters, K. Schuster, E. da Cunha, X. Fan, E. P. Farina, C. Mazzucchelli, H.-W. Rix, and A. Weiss, Copious amounts of dust and gas in a $z = 7.5$ quasar host galaxy, Astrophys. J. Lett. **851,** L8 (2017).

[15] P. Behroozi and J. Silk, The most massive galaxies and black holes allowed by ΛCDM, Mon. Not. R. Astron. Soc. **477,** 5382 (2018).

[16] J.-J. Tang, T. Goto, Y. Ohyama, C. Jin, C. Done, T.-Y. Lu, T. Hashimoto, E. Kilerci Eser, C.-Y. Chiang, and S. J. Kim, Rapid black hole growth at the dawn of the Universe: A super-Eddington quasar at $z = 6.6$, Mon. Not. R. Astron. Soc. **484,** 2575 (2019).

[17] R. Cecchi, M. Bolzonella, A. Cimatti, and G. Girelli, Quiescent galaxies at $z \gtrsim 2.5$: Observations versus models, Astrophys. J. **880,** L14 (2019).

[18] A. Smith and V. Bromm, Supermassive black holes in the early Universe, Contemp. Phys. **60,** 111 (2019).

[19] T. Wang *et al.*, A dominant population of optically invisible massive galaxies in the early Universe, Nature (London) **572,** 211 (2019).

[20] K. H. Seleim, A. A. El-Zant, and A. M. Abdel-Moneim, Enhanced spectrum of primordial perturbations, galaxy formation, and small-scale structure, Phys. Rev. D **102,** 063505 (2020).

[21] P. Colín, V. Avila-Reese, and O. Valenzuela, Substructure and halo density profiles in a warm dark matter cosmology, Astrophys. J. **542,** 622 (2000).

[22] P. Bode, J. P. Ostriker, and N. Turok, Halo formation in warm dark matter models, Astrophys. J. **556,** 93 (2001).

[23] A. V. Macciò, S. Paduroiu, D. Anderhalden, A. Schneider, and B. Moore, Cores in warm dark matter haloes: A catch 22 problem, Mon. Not. R. Astron. Soc. **424,** 1105 (2012).

[24] M. R. Lovell, C. S. Frenk, V. R. Eke, A. Jenkins, L. Gao, and T. Theuns, The properties of warm dark matter haloes, Mon. Not. R. Astron. Soc. **439,** 300 (2014).

[25] A. El-Zant, S. Khalil, and A. Sil, Warm dark matter in a B-L inverse seesaw scenario, Phys. Rev. D **91,** 035030 (2015).

[26] D. N. Spergel and P. J. Steinhardt, Observational Evidence for Self-Interacting Cold Dark Matter, Phys. Rev. Lett. **84,** 3760 (2000).

[27] A. Burkert, The structure and evolution of weakly self-interacting cold dark matter halos, Astrophys. J. **534,** L143 (2000).

[28] C. S. Kochanek and M. White, A quantitative study of interacting dark matter in halos, Astrophys. J. **543,** 514 (2000).

[29] J. Miralda-Escudé, A test of the collisional dark matter hypothesis from cluster lensing, Astrophys. J. **564,** 60 (2002).

[30] J. Zavala, M. Vogelsberger, and M. G. Walker, Constraining self-interacting dark matter with the Milky Way's dwarf spheroidals, Mon. Not. R. Astron. Soc. **431,** L20 (2013).

[31] O. D. Elbert, J. S. Bullock, S. Garrison-Kimmel, M. Rocha, J. Oñorbe, and A. H. G. Peter, Core formation in dwarf haloes with self-interacting dark matter: No fine-tuning necessary, Mon. Not. R. Astron. Soc. **453,** 29 (2015).

[32] J. Fan, A. Katz, L. Randall, and M. Reece, Double-disk dark matter, Phys. Dark Universe **2,** 139 (2013).

[33] L. Randall and J. Scholtz, Dissipative dark matter and the Andromeda plane of satellites, J. Cosmol. Astropart. Phys. 09 (2015) 057.

[34] R. Foot and S. Vagnozzi, Dissipative hidden sector dark matter, Phys. Rev. D **91,** 023512 (2015).

[35] R. Foot and S. Vagnozzi, Solving the small-scale structure puzzles with dissipative dark matter, J. Cosmol. Astropart. Phys. 07 (2016) 013.

[36] J. Goodman, Repulsive dark matter, New Astron. **5,** 103 (2000).

[37] W. Hu, R. Barkana, and A. Gruzinov, Fuzzy Cold Dark Matter: The Wave Properties of Ultralight Particles, Phys. Rev. Lett. **85,** 1158 (2000).

[38] H.-Y. Schive, M.-H. Liao, T.-P. Woo, S.-K. Wong, T. Chiueh, T. Broadhurst, and W.-Y. P. Hwang, Understanding the Core-Halo Relation of Quantum Wave Dark Matter from 3D Simulations, Phys. Rev. Lett. **113,** 261302 (2014).

[39] D. J. E. Marsh and J. Silk, A model for halo formation with axion mixed dark matter, Mon. Not. R. Astron. Soc. **437,** 2652 (2014).

[40] L. Hui, J. P. Ostriker, S. Tremaine, and E. Witten, Ultralight scalars as cosmological dark matter, Phys. Rev. D **95,** 043541 (2017).

[41] M. Li, X.-D. Li, S. Wang, and Y. Wang, Dark energy, Commun. Theor. Phys. **56,** 525 (2011).

[42] J. Yoo and Y. Watanabe, Theoretical models of dark energy, Int. J. Mod. Phys. D **21,** 1230002 (2012).

[43] P. Brax, What makes the Universe accelerate? A review on what dark energy could be and how to test it, Rep. Prog. Phys. **81,** 016902 (2018).

[44] A. Kamenshchik, U. Moschella, and V. Pasquier, An alternative to quintessence, Phys. Lett. B **511,** 265 (2001).

[45] M. C. Bento, O. Bertolami, and A. A. Sen, Generalized Chaplygin gas, accelerated expansion, and dark-energy-matter unification, Phys. Rev. D **66,** 043507 (2002).

[46] W. Yang, S. Pan, S. Vagnozzi, E. Di Valentino, D. F. Mota, and S. Capozziello, Dawn of the dark: Unified dark sectors

and the EDGES Cosmic Dawn 21-cm signal, J. Cosmol. Astropart. Phys. 11 (2019) 044.

[47] R. Jackiw, A particle field theorist's lectures on supersymmetric, non-Abelian fluid mechanics and d-branes, arXiv:physics/0010042.

[48] V. Gorini, A. Kamenshchik, U. Moschella, and V. Pasquier, The Chaplygin gas as a model for dark energy, in *The Tenth Marcel Grossmann Meeting: On Recent Developments in Theoretical and Experimental General Relativity Gravitation and Relativistic Field Theories (In 3 Volumes)* (World Scientific, Singapore, 2005), pp. 840–859.

[49] H. B. Sandvik, M. Tegmark, M. Zaldarriaga, and I. Waga, The end of unified dark matter?, Phys. Rev. D **69,** 123524 (2004).

[50] L. M. Beça, P. P. Avelino, J. P. de Carvalho, and C. J. Martins, Role of baryons in unified dark matter models, Phys. Rev. D **67,** 101301 (2003).

[51] J. C. Fabris, S. V. B. Gonçalves, H. E. S. Velten, and W. Zimdahl, Matter power spectrum for the generalized Chaplygin gas model: The Newtonian approach, Phys. Rev. D **78,** 103523 (2008).

[52] V. Gorini, A. Y. Kamenshchik, U. Moschella, O. F. Piattella, and A. A. Starobinsky, Gauge-invariant analysis of perturbations in Chaplygin gas unified models of dark matter and dark energy, J. Cosmol. Astropart. Phys. 02 (2008) 016.

[53] J. C. Fabris, H. E. S. Velten, and W. Zimdahl, Matter power spectrum for the generalized Chaplygin gas model: The relativistic case, Phys. Rev. D **81,** 087303 (2010).

[54] C.-G. Park, J.-C. Hwang, J. Park, and H. Noh, Observational constraints on a unified dark matter and dark energy model based on generalized Chaplygin gas, Phys. Rev. D **81,** 063532 (2010).

[55] Y. Wang, D. Wands, L. Xu, J. De-Santiago, and A. Hojjati, Cosmological constraints on a decomposed Chaplygin gas, Phys. Rev. D **87,** 083503 (2013).

[56] R. R. Reis, I. Waga, M. O. Calvão, and S. E. Jorás, Entropy perturbations in quartessence Chaplygin models, Phys. Rev. D **68,** 061302 (2003).

[57] W. Zimdahl and J. C. Fabris, Chaplygin gas with non-adiabatic pressure perturbations, Classical Quantum Gravity **22,** 4311 (2005).

[58] N. Bilic, G. B. Tupper, and R. D. Viollier, Chaplygin gas cosmology—unification of dark matter and dark energy, J. Phys. A **40,** 6877 (2007).

[59] P. P. Avelino, K. Bolejko, and G. F. Lewis, Nonlinear Chaplygin gas cosmologies, Phys. Rev. D **89,** 103004 (2014).

[60] This ignores the baryon contribution, as the whole matter density is supposed to emanate from the unified dark matter component. The effect of baryons generally alleviates the problems addressed here [50]; any solution to these problems that is effective in their absence should remain valid when they are added.

[61] A. Lewis and A. Challinor, Code for anisotropies in the microwave background, https://camb.info/.

[62] J. A. Peacock, *Cosmological Physics,* edited by John A. Peacock (Cambridge University Press, Cambridge, England, 1999), p. 704, ISBN 052141072X.

[63] N. Bilić, R. J. Lindebaum, G. B. Tupper, and R. D. Viollier, Nonlinear evolution of dark matter and dark energy in the

Chaplygin-gas cosmology, J. Cosmol. Astropart. Phys. 11 (2004) 008.

[64] J. A. Fillmore and P. Goldreich, Self-similar gravitational collapse in an expanding universe, Astrophys. J. **281,** 1 (1984).

[65] R. Fernandes, J. De Carvalho, A. Y. Kamenshchik, U. Moschella, and A. da Silva, Spherical "top-hat" collapse in general-Chaplygin-gas-dominated universes, Phys. Rev. D **85,** 083501 (2012).

[66] D. Serre, Multidimensional shock interaction for a Chaplygin gas, Arch. Ration. Mech. Anal. **191,** 539 (2009).

[67] G. Wang, The Riemann problem for one dimensional generalized Chaplygin gas dynamics, J. Math. Anal. Appl. **403,** 434 (2013).

[68] H. Yang and Y. Zhang, New developments of delta shock waves and its applications in systems of conservation laws, J. Differ. Equ. **252,** 5951 (2012).

[69] J. E. Gunn, I. Gott, and J. Richard, On the infall of matter into clusters of galaxies and some effects on their evolution, Astrophys. J. **176,** 1 (1972).

[70] A. Loeb, First light, arXiv:astro-ph/0603360.

[71] D. Rubin and A. Loeb, The virialization density of peaks with general density profiles under spherical collapse, J. Cosmol. Astropart. Phys. 12 (2013) 019.

[72] E. O. Nadler *et al.* (DES Collaboration), Milky Way satellite census. II. Galaxy-halo connection constraints including the impact of the large magellanic cloud, Astrophys. J. **893,** 48 (2020).

[73] For simplicity, we ignore here the baryon contribution, which will be included in the comparison with observation in the following subsection.

[74] D. M. Scolnic *et al.* (Pan-STARRS1 Collaboration), The complete light-curve sample of spectroscopically confirmed SNe Ia from Pan-STARRS1 and cosmological constraints from the combined pantheon sample, Astrophys. J. **859,** 101 (2018).

[75] D. Scolnic *et al.*, The Pantheon + analysis: The full dataset and light-curve release, arXiv:2112.03863.

[76] S. Alam, F. D. Albareti, C. A. Prieto, F. Anders, S. F. Anderson, T. Anderton, B. H. Andrews, E. Armengaud, É. Aubourg, S. Bailey *et al.*, The eleventh and twelfth data releases of the Sloan Digital Sky Survey: Final data from SDSS-III, Astrophys. J. Suppl. Ser. **219,** 12 (2015).

[77] J. Magana, M. H. Amante, M. A. Garcia-Aspeitia, and V. Motta, The Cardassian expansion revisited: Constraints from updated Hubble parameter measurements and type Ia supernova data, Mon. Not. R. Astron. Soc. **476,** 1036 (2018).

[78] P. A. R. Ade *et al.* (Planck Collaboration), Planck 2015 results. XIV. Dark energy and modified gravity, Astron. Astrophys. **594,** A14 (2016).

[79] Z. Zhai, C.-G. Park, Y. Wang, and B. Ratra, CMB distance priors revisited: Effects of dark energy dynamics, spatial curvature, primordial power spectrum, and neutrino parameters, J. Cosmol. Astropart. Phys. 07 (2020) 009.

[80] L. Chen, Q.-G. Huang, and K. Wang, Distance priors from Planck final release, J. Cosmol. Astropart. Phys. 02 (2019) 028.

[81] J. Lesgourgues, The cosmic linear anisotropy solving system (CLASS) I: Overview, arXiv:1104.2932.

[82] D. Foreman-Mackey, D. W. Hogg, D. Lang, and J. Goodman, EMCEE: The MCMC hammer, Publ. Astron. Soc. Pac. **125,** 306 (2013).

[83] A. El-Zant, W. El Hanafy, and S. Elgammal, H_0 tension and the phantom regime: A case study in terms of an infrared $f(T)$ gravity, Astrophys. J. **871,** 210 (2019).

[84] A. G. Riess, S. Casertano, W. Yuan, J. B. Bowers, L. Macri, J. C. Zinn, and D. Scolnic, Cosmic distances calibrated to 1% precision with Gaia EDR3 parallaxes and Hubble space telescope photometry of 75 Milky Way cepheids confirm tension with ΛCDM, Astrophys. J. Lett. **908,** L6 (2021).

[85] E. O. Nadler *et al.* (DES Collaboration), Constraints on Dark Matter Properties from Observations of Milky Way Satellite Galaxies, Phys. Rev. Lett. **126,** 091101 (2021).

[86] E. O. Nadler, S. Birrer, D. Gilman, R. H. Wechsler, X. Du, A. Benson, A. M. Nierenberg, and T. Treu, Dark matter constraints from a unified analysis of strong gravitational lenses and Milky Way satellite galaxies, Astrophys. J. **917,** 7 (2021).

[87] A. A. El-Zant, Unified dark matter: Constraints from galaxies and clusters, Mon. Not. R. Astron. Soc. **453,** 2251 (2015).